

Congenital foot deformation alters the topographic organization in the primate somatosensory system

Chia-Chi Liao · Hui-Xin Qi · Jamie L. Reed ·

Daniel J. Miller · Jon H. Kaas

Received: 20 August 2014 / Accepted: 7 October 2014

© Springer-Verlag Berlin Heidelberg 2014

Abstract Limbs may fail to grow properly during fetal development, but the extent to which such growth alters the nervous system has not been extensively explored. Here we describe the organization of the somatosensory system in a 6-year-old monkey (*Macaca radiata*) born with a deformed left foot in comparison to the results from a normal monkey (*Macaca fascicularis*). Toes 1, 3, and 5 were missing, but the proximal parts of toes 2 and 4 were present. We used anatomical tracers to characterize the patterns of peripheral input to the spinal cord and brainstem, as well as between thalamus and cortex. We also determined the somatotopic organization of primary somatosensory area 3b of both hemispheres using multiunit electrophysiological recording. Tracers were subcutaneously injected into matching locations of each foot to reveal their representations within the lumbar spinal cord, and the gracile nucleus (GrN) of the brainstem. Tracers injected into the representations of the toes and plantar pads of cortical area 3b labeled neurons in the ventroposterior lateral nucleus (VPL) of the thalamus. Contrary to the orderly arrangement of the foot representation throughout the lemniscal pathway in the normal monkey, the plantar representation of the deformed foot was significantly expanded and intruded into the expected representations of toes in the spinal cord, GrN, VPL, and area 3b. We also observed abnormal representation of the intact foot in the ipsilateral spinal cord and contralateral area 3b. Thus, congenital malformation influences the somatotopic representation of the deformed as well as the intact foot.

Keywords Congenital limb deficiency · Macaque · Somatotopy · Plasticity · Reorganization

Introduction

As estimated by the Centers for Disease Control and Prevention (2011), each year 1 in 2,500 infants are born with a malformed extremity in the United States. This so-called congenital limb deficiency typically involves missing part of a finger or the absence of an arm(s) or leg(s). The failure to fully develop a limb may result from either the genetic arrest of fetal development or environment factors such as amniotic band constriction or hazardous chemical or radiation exposures during the first gestation trimester (Dy et al. 2014; Ogino 2007; Goldman 1980). Over the past few decades, efforts to improve the function and physical appearance of deficient limbs have resulted in significant progress (Wall et al. 2013; Gabos 2006). However, we are still limited in our understanding of how the somatosensory system is organized and functions in the absence of normal limb development.

A mainstay of the mammalian somatosensory system is the systematic and topographic representation of the body surface along the lemniscal pathway beginning in the spinal cord and continuing on up to the first cortical target area, the primary somatosensory cortex (or area 3b in primates). It is generally thought that development of the topographic representation of somatosensory input (somatotopy), especially in the cortex is shaped by molecular gradients and refined in the typical Hebbian fashion by patterns of impulses arising from the periphery during a critical window of postnatal development (Killackey et al. 1995; Kaas and Catania 2002; Sperry 1963; van der Loos and Dorfl 1978; Luo and Flanagan 2007; Lokmane et al.

C.-C. Liao (✉) · H.-X. Qi · J. L. Reed ·
D. J. Miller · J. H. Kaas
301 Wilson Hall, Department of Psychology, Vanderbilt
University, 111 21st Avenue South, Nashville, TN 37212, USA
e-mail: chia-chi.liao@vanderbilt.edu

2013; Hubel and Wiesel 1970; Constantine-Paton and Law 1982). The boundaries of the representations of individual body parts are thus modulated by the strengths of inputs and the use of body parts during development and to a limited extent throughout life (Kaas et al. 2008; Blake et al. 2002; Krubitzer and Dooley 2013). Accordingly, how the nervous system develops somatotopy at various levels along the ascending pathway is of interest in the case of congenital limb deficiency since the brain is never driven by the inputs from the missing limb, which may alter the development of somatotopy in the nervous system. The topic has been briefly explored in human studies by non-invasive imaging approaches such as electroencephalography (EEG), magnetoencephalography (MEG) and functional magnetic resonance imaging (fMRI) techniques (Flor et al. 1995, 1998; Montoya et al. 1998; Stoeckel et al. 2005a, b). Nevertheless, the spatial resolution of these imaging methods did not provide a sufficiently detailed somatotopic map to resolve the question of whether large-scale reorganization occurs or not in the somatosensory system of patients born with limb malformations. Methodological issues further limit research into the alteration of somatosensory representations at subcortical levels, including modifications to connections between levels along the lemniscal pathway.

Here we had the unique opportunity to study the foot representation at multiple levels of the somatosensory system in an adult macaque monkey (6 years) born with an intact right foot but missing toes on the left foot. The representation of the plantar pads in the spinal cord and GrN on each side of the body was revealed by subcutaneous injections of cholera toxin subunit B (CTB) conjugated with horseradish peroxidase (B-HRP) into matching locations of the feet. Microelectrode recordings were used to map the foot representation of area 3b in both hemispheres. We then injected CTB and wheat germ agglutinin horseradish peroxidase (WGA-HRP) into functionally defined representations of the plantar pads and toes in cortical area 3b to identify the thalamocortical projections from VPL. Cytochrome oxidase (CO), Nissl or vesicular glutamate transporter 2 (VGLUT2) staining was employed to reveal the architecture of somatosensory nuclei in the brainstem and thalamus. This research strategy was repeated in one normal macaque monkey for comparison. Our primary goal was to determine whether the congenital absence of toes altered the foot representation along the lemniscal pathway from spinal cord to cortex. Our second goal was to see if the failure to fully develop one foot affected the somatotopy of the lemniscal pathway unilaterally or bilaterally, given that the unilateral pathway interacts callosally in cortex, and that the incomplete development of one foot may alter the use of the other foot and thus modify somatosensory connections in a Hebbian

fashion. Given the topography and connectivity of the somatosensory system in macaques monkeys with (Florence and Kaas 1995; Pons et al. 1991; Merzenich et al. 1984; Jain et al. 2008; Florence et al. 1996) and without therapeutic amputations (Nelson et al. 1980; Qi and Kaas 2006; Rausell et al. 1998; Jones 2007; Mayner and Kaas 1986), we compared the scope of reorganization across groups. Our results demonstrated that congenital foot malformation resulted in significant reorganization of the representation of the toes and plantar pads along the somatosensory pathway. Alterations not only occurred in the ipsilateral spinal cord, GrN, and contralateral thalamus and cortex that represent the deformed foot, but also in the spinal cord and cortex representing the intact foot.

Materials and methods

One long-tailed macaque (*Macaca fascicularis*; MM-N) and one bonnet macaque monkey (*Macaca radiata*; MM-D) were used in this study. Previous studies have not revealed notable differences in the somatotopic organization in the thalamus and area 3b in these two species (Nelson and Kaas 1981; Nelson et al. 1980; Padberg and Krubitzer 2006; Jones and Friedman 1982). MM-D was born with a deformed left foot (Fig. 1; Hendrickx and Prahalada 1986). Toes 1, 3, and 5 were absent but the

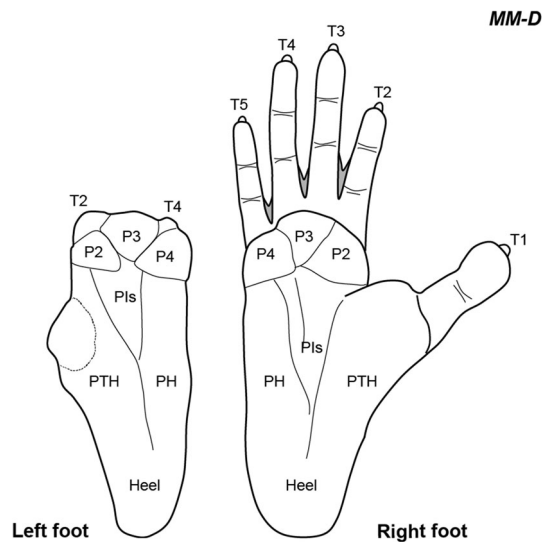


Fig. 1 Drawings made from photographs of a macaque monkey with a congenitally deformed foot (MM-D) show the structure of the glabrous surface of the feet. The foot on the right side was normal in appearance with intact toes 1–5 and plantar pads. Toe webs were present between the toes (gray shading). On the left foot, toes 1, 3, and 5 were congenitally absent but the most proximal nubs of toes 2 and 4 and the plantar pad remained intact. T1–T5 toes 1–5, P2–P4 plantar pads 2–4, PH hypotenar pad, P1s insular plantar pads, PTH thenar pad

proximal portions of toes 2 and 4 and the plantar pads remained intact. Toes 1–5 and the plantar pads on the right foot appeared normal. All animal care and surgical procedures were performed in accordance with the Guide for the Care and Use of Laboratory Animals established by National Institutes of Health and approved by the Animal Care and Use Committee of Vanderbilt University.

Subcutaneous tracer injections

Animals were sedated by an intramuscular (IM) injection of ketamine hydrochloride (10 mg/kg) and transitioned to the inhaled anesthetic isoflurane (1–2 %) in oxygen. We injected a transganglionic tracer, B-HRP (0.2 % in distilled H₂O, List Biological), into the plantar pad 3 (P3) and thenar pad (PTH) of both feet. Injections of 5 µl of B-HRP solution were made twice at each location. Five days were allowed for tracer transportation before a terminal mapping procedure.

Terminal microelectrode mapping and tracer injections

Surgical procedures

The animal was initially tranquilized with an injection of ketamine hydrochloride (10–25 mg/kg) and the anesthesia was maintained at a surgical level with 1–3 % isoflurane. While fully anesthetized, animals were placed on the stereotaxic apparatus. Vital signs including heart rate, blood pressure, respiration rate, expiration CO₂, arterial O₂ saturation, and body temperature were monitored throughout the procedure. Bilateral craniotomies were performed over the parietal cortex to expose the foot representations in area 3b, which is directly adjacent to the central sulcus on the brain surface and extends medially into the longitudinal fissure in macaque monkeys (Nelson et al. 1980). The dura was removed for microelectrode penetrations. A print of an enlarged photo of the exposed brain surface was used to guide and record the sites of microelectrode penetrations and tracer injections.

Multiunit microelectrode mapping and tracer injections

Transition between inhaled isoflurane (1–2 %) and intravenous infusion of ketamine hydrochloride (12 mg/kg/h) occurred immediately prior to electrophysiological recording. Xylazine (0.4 mg/kg, IM) was given as needed. Previous studies in macaque monkeys (Nelson et al. 1980) guided our mapping. Area 3b adjoins the rostral area 3a and the caudal area 1 with reversals of body representations. The borders of area 3b were also determined based upon the neuron's receptive field using standard mapping methods such as lightly touching with fine probes,

brushing, and tapping. Neurons in area 3b have small, discrete receptive fields and are sensitive to low threshold, cutaneous stimulation. Area 3a neurons are distinguished by a tendency to respond to tapping and muscle or joint manipulations. A low-impedance tungsten microelectrode (1 MΩ) was lowered perpendicularly through the cortical surface to a depth of 650 µm where the middle layers of cortex were located to map receptive fields. This electrode placement strategy was repeated every 350–500 µm across the surface of the brain to obtain the foot representations of area 3b in parietal cortex of both hemispheres. Somatotopic maps of the lateral surface of parietal cortex were first determined for the purpose of tracer injections. Two neuroanatomical tracers including WGA-HRP (1 % in distilled H₂O; Vector Laboratories, Burlingame, CA, USA) and CTB (Sigma, St. Louis, MO, USA) were used. All injections were made with 1-µl Hamilton Syringes outfitted with glass pipettes drawn to fine tips (25–50 µm). To ensure tracers involved the granular cortical layers, which receive feedforward projections from the thalamus, one injection was placed at a depth of 800 µm, and a second injection was placed at 600 µm. Micropipettes were kept in position for 2–5 min after each injection to minimize backflow. After tracers were deposited, the exposed brain surfaces were protected with a thin layer of silicon oil for the remaining electrophysiological mapping.

In addition to the recordings on the lateral surface of the parietal cortex, microelectrodes were lowered for deep penetrations in the medial walls of the longitudinal fissure to map the medial aspect of the foot representations. The receptive fields were systematically determined every 300 µm (depth) until no responses to lower limbs were detected. Finally, we marked the borders of area 3b by small electrolytic lesions identifiable after post-mortem tissue processing.

Perfusion and histology

At the conclusion of mapping, animals were deeply anesthetized with a lethal dose of sodium pentobarbital (120 mg/kg). Perfusion was initiated through the ascending aorta with phosphate-buffered saline (PBS, pH 7.4) and continued with 4 % paraformaldehyde in phosphate buffer and 10 % sucrose in fixative. The brain and spinal cord were extracted and immersed in 30 % sucrose in PBS overnight at 4 °C for cryoprotection. The brain was cut in the coronal plane at a thickness of 50 µm and the spinal cord was cut in the horizontal plane at a thickness of 40 µm on a freezing microtome.

Sections were saved in series for different histological purposes. From the first block of sections, including bilateral neocortex and thalamus, two series were

processed with standard immunohistochemical procedures for CTB (Angelucci et al. 1996) and WGA-HRP with 3,3,5,5-tetramethylbenzidine (TMB; Gibson et al. 1984) to reveal cortical projection neurons in the thalamus. One set of the brainstem and spinal cord sections were processed with TMB reaction to visualize labeled plantar afferents in the spinal cord and the GrN. Tissue was processed for CO and Nissl staining in two separate series to reveal cortical and thalamic architectures as previously described (Qi et al. 2011b; Wong-Riley 1979). The sections processed for the VGLUT2 used a mouse monoclonal anti-VGLUT2 primary antibody (Millipore, Billerica, MA, USA), which was characterized in previous publications (Balaram et al. 2013; Liao et al. 2013).

Data analysis

Measures of labeled plantar afferents

We examined the labeled profiles resulting from tracer injections using an upright bright/darkfield microscope (Nikon E800 microscope) outfitted with a Nikon DXM 1200 camera. The labeled profiles were imaged and imported to Adobe Photoshop CS6 (Adobe Systems, San Jose, CA, USA) for brightness and contrast adjustment. Subcutaneous injections of B-HRP into P3 and PTH on both feet revealed how the plantar afferents terminate in the GrN through the lumbar spinal cord.

Photomicrographs of the B-HRP-labeled profiles were taken under the same lighting using darkfield microscopy, and then converted to 8-bit gray scale images for measurement. The ImageJ 64 program (National Institutes of Health, Bethesda, MD, USA) was used to analyze the labeled areas and optical densities between two sides in the spinal cord and brainstem from a series of sections within one monkey (see p. 13664 in Materials and method by Qi et al. 2011a). The purpose of the statistical comparison was to support the visual evidence that the labeled regions are or are not different between the two sides in the same animal and not to make inferences about a population of macaque monkeys. In brief, after converting each image to grayscale, the threshold was adjusted to appropriately select the B-HRP-labeled foci across rostrocaudal sections. The area of the B-HRP-labeled field was calculated by converting the total number of labeled pixels into square millimeters. The depth of staining intensity (the grayscale value corresponding to the optical density) was normalized into percentages (0–100 %) to facilitate comparison between cases. The areas and optical densities of the B-HRP-labeled regions in the spinal cord and brainstem on the two sides were statistically compared using the Wilcoxon matched-pairs signed-rank test (GraphPad InStat software). Values of $P < 0.05$ were considered statistically

significant. Data are reported as mean \pm standard error of the mean (SEM).

Distribution of thalamocortical projection neurons

We examined the distributions of labeled neurons in the VPL from injections to the representations of the toes and plantar pads in cortical area 3b. The locations of WGA-HRP- and CTB-labeled neurons in the VPL were plotted using the Neurolucida system (MBF Bioscience, Williston, VT, USA). Special care was taken to mark blood vessels, anatomical landmarks, and electrolytic lesions for the alignment of plots and architectures in adjacent CO, VGLUT2, CTB, and WGA-HRP sections in Adobe Illustrator CS6.

Foot representations in the cortex

Based on the receptive fields and response modalities identified by the electrophysiological recordings, the foot representation in the cortex was reconstructed in Adobe Illustrator CS6. In short, we scanned and imported the printed photo of the exposed cortex that was marked with locations of microelectrode penetrations to the Adobe Illustrator and reconstructed the map accordingly. The recording sites of the deep penetrations along the medial wall of the cerebral hemisphere were reconstructed based on the depths recorded during the electrophysiological mapping.

Results

In the present study, we identified the somatotopic organization of representations of both feet at multiple levels along the lemniscal pathway in a macaque monkey that was born with one normal appearing foot, and one foot for which toes failed to develop (Fig. 1). In order to facilitate this comparison, we described the representations of the glabrous foot at individual levels in a normal monkey (MM-N) and in the monkey with a congenital foot deficiency (MM-D). Anatomical tracing and electrophysiological mapping were used to reveal the foot representations in the spinal cord, dorsal column nuclei, thalamus, and cortex on both sides of the nervous system.

Spinal cord

The spinal cord is the first station where sensory afferents enter the central nervous system. Some of the primary afferents form synapses on the second-order spinal neurons in the dorsal horn of the spinal cord, and other fibers travel in the dorsal columns and terminate in the

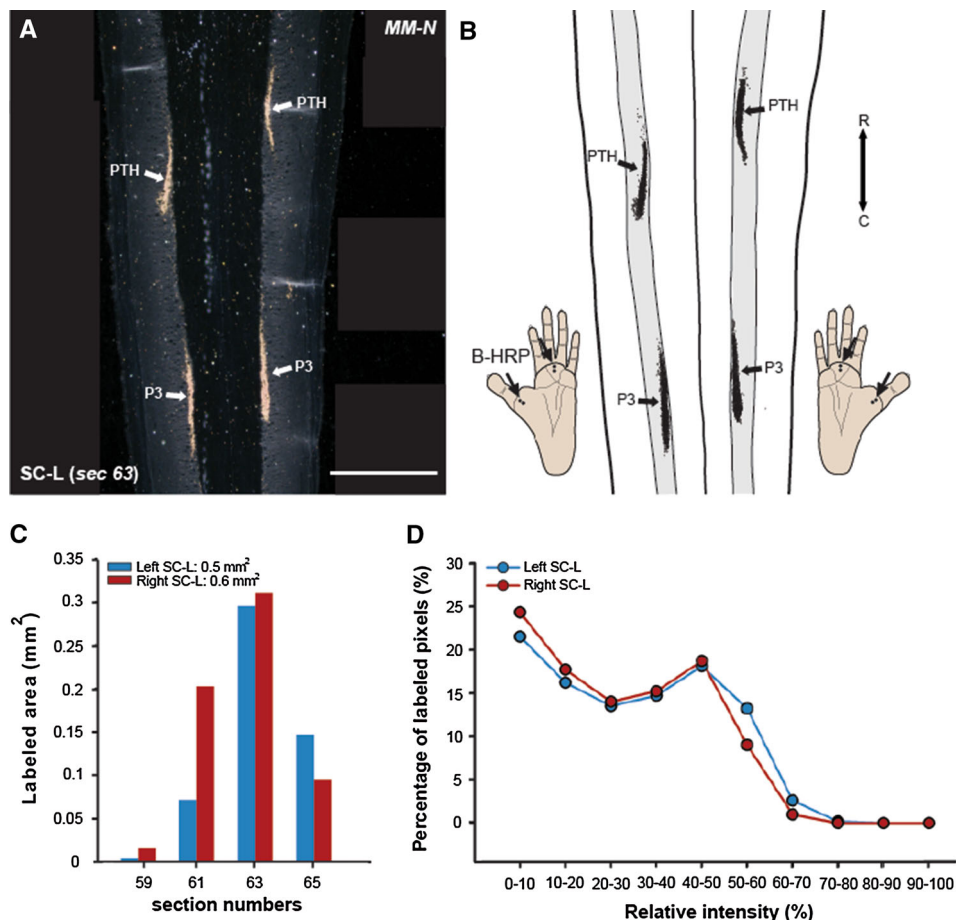


Fig. 2 Axonal terminations in the spinal cord labeled by subcutaneous injections of cholera toxin subunit B (CTB) conjugated with horseradish peroxidase (B-HRP) in matching locations of P3 and PTH in both feet of a normal macaque monkey (MM-N) are similar. **a** Dark-field photomicrograph of one horizontal section shows the B-HRP-labeled terminals (arrows) in the dorsal horn gray matter of lumbar spinal cord. Two dense and widely separated patches of labeled axonal terminals are arranged along the medial regions of spinal cord on the two sides. **b** Alignment of plots of four consecutive sections shows the B-HRP-labeled fields in the dorsal horn gray matter on the two sides of spinal cord are similar in size and intensity.

c Bar graphs show the area of B-HRP-labeled fields in the dorsal horn of spinal cord on the two sides across the four sections. The values obtained from quantitative measurement using ImageJ64 (0.5 mm^2 left side, 0.6 mm^2 right side) did not show significant differences in the extent of labeled fields in the spinal cord on the two sides ($P = 0.625$; Wilcoxon matched-pairs signed-rank test). **d** Curve diagram showing that the percentages of relative intensities of labeled pixels in the spinal cord on each side are similar ($P = 0.571$ by Wilcoxon matched-pairs signed-rank test). C caudal, R rostral. Scale bar in **a** is 1 mm

brainstem (Abraira and Ginty 2013; Willis 2008). In previous studies, we have demonstrated that subcutaneous injections of tracers into the matching locations of the two hands produced foci of labeled axon terminals on both sides of the spinal cord in a symmetric and comparable pattern in monkeys (Qi et al. 2011a, 2013, 2014b), suggesting that the somatotopic organization is similar in the spinal cord on both sides. To compare the plantar projections in the spinal cord on the two sides, we injected the same amounts of B-HRP to matching locations on P3 and PTH in both feet of each animal and then sectioned the lumbar region of the spinal cord in a horizontal plane. In the normal monkey MM-N, two dense and widely

separated patches of labeled axonal terminals were present along the most medial aspects of the spinal cord gray matter on each side (Fig. 2a). The B-HRP-labeled fields extended dorsoventrally about 250 μm within the dorsal horn on both sides. Although B-HRP was injected into matching locations on each foot, labeled loci were not within perfectly symmetrical rostrocaudal domains of the spinal cord; the loci of labeled cells on the right side were slightly more rostral than the labeled cells on the left side. Such slight differences in the level of peripheral nerve inputs to the dorsal horn indicate that some variability may occur naturally in normal monkeys (e.g. Florence et al. 1988). Plots of four consecutive sections from the

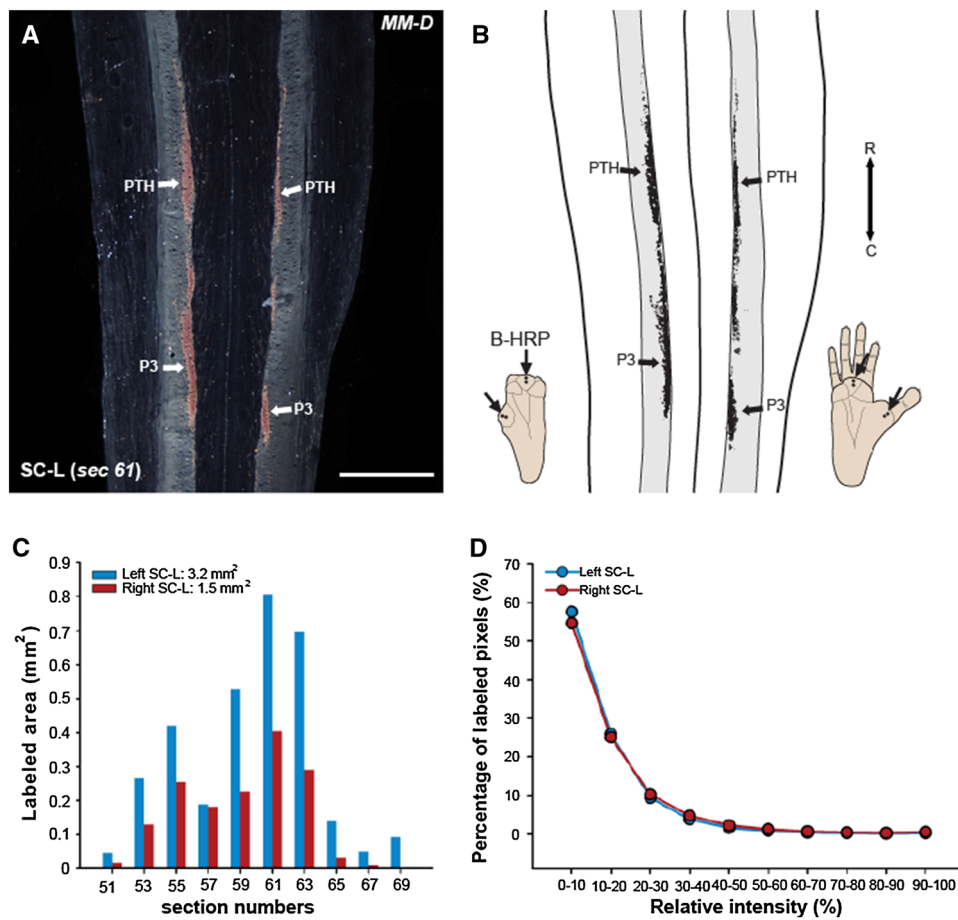


Fig. 3 Axonal terminations in the spinal cord labeled by subcutaneous B-HRP injections in matching locations of P3 and PTH in both feet of a macaque monkey with a congenitally deformed left foot (MM-D) differ on the two sides and from the normal pattern. **a** Dark-field photomicrograph of one *horizontal* section shows the B-HRP-labeled terminals in the dorsal horn of lumbar spinal cord. Three labeled patches were apparent along the medial aspect of the spinal cord grey matter on the *right* side, where represents the normal appearing foot. The matching injections in the deformed foot labeled one dense patch rostrally and two closely arranged patches caudally on the *left* side. **b** Alignment of plots of four consecutive sections

shows that the B-HRP-labeled patches in the dorsal horn gray matter on the two sides fused rostrocaudally. The labeled fields on the *left* side expanded rostrocaudally and laterally when compared to the *right* side. **c** Bar graphs show the areal extents of B-HRP-labeled fields in the dorsal horn of spinal cord on the two sides across ten sections. The total labeled area is 3.2 mm^2 on the *left* side and 1.5 mm^2 on the *right* side. The extent of B-HRP-labeled terminals is significantly expanded on the *left* side ($*P = 0.002$). **d** Curve diagram shows that the percentages of relative intensities of labeled pixels in the spinal cord on the two sides are similar ($P = 0.3223$). Scale bar in **a** is 1 mm

B-HRP series containing the dorsal horn of the spinal cord were overlaid in Fig. 2b to show how similar the labeled fields were in terms of the size of the loci and the intensity on both sides. To quantitatively evaluate whether the plantar projections from both feet terminated in the spinal cord in a similar pattern, we analyzed the area and optical density of B-HRP-labeled terminal fields on each side across adjacent sections using ImageJ64 (Fig. 2c). The areas of each of the B-HRP-labeled fields were similar: 0.5 mm^2 on the *left* side and 0.6 mm^2 on the *right* side. No significant differences were detected in the area ($P = 0.625$) or optical densities ($P = 0.571$) of the B-HRP-labeled fields of the both sides.

The same strategy was used to examine the plantar projections to the spinal cord of the monkey with the deformed foot, MM-D (Fig. 3). The B-HRP injections in P3 and PTH of the intact foot formed three patches of labeled terminals along the most medial region of the spinal cord gray matter on the *right* side. Sparse amounts of B-HRP-labeled terminals were noted between the patches (Fig. 3b). Thus, the sensory projections to the dorsal horn from the normal appearing foot in this case were more spread out than in normal monkeys. The matched B-HRP injections in the deformed foot labeled one dense patch rostrally and two closely arranged patches caudally in the spinal cord. The three patches fused and expanded

rostrocaudally and laterally when compared to the labeled patches on the contralateral side. Thus, the B-HRP-labeled axons extended dorsoventrally about 750 µm on the left side for the deformed foot and about 650 µm on the right side for the normal appearing foot. Quantification of the area and optical density of the B-HRP-labeled patterns of axon terminals in the spinal cord on both sides revealed that the labeled area on the left side (3.2 mm^2 in total) was significantly larger than the labeled area on the right (1.5 mm^2 in total; $P = 0.002$), while the labeled optical densities were statistically indistinguishable ($P = 0.3223$; Fig. 3c, d).

In summary, the results indicate that the distributions of inputs from the plantar area of the foot were abnormal in both the deformed foot with missing toes and the normal-appearing foot in case MM-D. The inputs from the PTH and P3 were segregated on both sides of the spinal cord in the normal monkey, MM-N, while they were spread out and nearly continuous on each side of the spinal cord in the monkey with a deformed foot, MM-D. However, the widespread distributions of inputs were greater from the deformed foot.

Brainstem

In normal monkeys, the GrN contains dark CO patches that correspond to cellular aggregations receiving projections from individual subdivisions of the foot (Qi and Kaas 2006). The glabrous toes are represented from the tibial toe 1 to the fibular toe 5 in a ventral to dorsal series of CO patterns close to the medial margin of GrN, while the plantar pads follow in a matching but more medial sequence of patterns, with that from PTH ventral to P3. A narrow most medial portion of GrN, sometimes described as a separate nucleus, represents the tail. The most lateral parts of GrN are devoted to the ankle, and lower and then upper leg.

Some of these aspects of GrN organization are shown for our normal monkey in Fig. 4. The patchy appearance of GrN and the adjoining cuneate nucleus, CuN, is shown in Fig. 4a, where the GrN on the right is slightly more rostral than the GrN on the left. On each side the expected location for the representations of toes is outlined, and as PTH and P3 of the plantar foot were injected with B-HRP in this monkey, label was transported to the expected locations in GrN next to the representations of toes with the label from PTH ventral (on the right) and lateral (on the left) to the label from P3. Other aspects of the normal organization of GrN are illustrated in Fig. 5. In Fig. 5a, the locations of the labeled axon terminals in GrN are shown for a series of sections from 0.9 mm caudal to the obex to 0.1 mm rostral to the obex, thus covering most of the length of GrN. In these sections, two or more patches of labeled axons are visible, with the more ventral patches for PTH and the

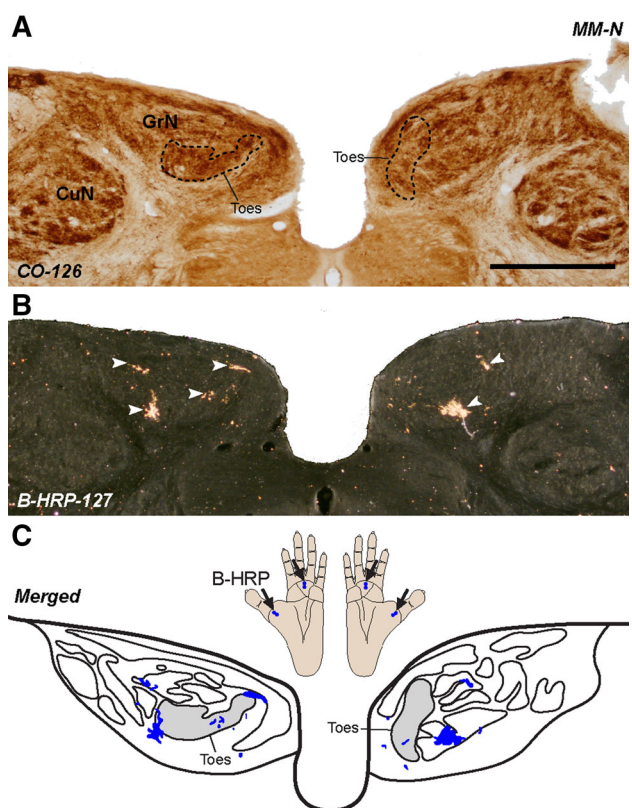


Fig. 4 Photomicrographs of a normal macaque monkey (MM-N) illustrate typical topographic organization of the foot representation in the gracile nucleus (GrN). **a** Photomicrograph of a coronal section reacted for cytochrome oxidase (CO) shows the CO-cluster patterns in the GrN. The CO-dense patches (*dashed outline*) in the medioventral region correspond to the representations of toes and in the lateral region correspond to the representations of plantar pads, with the PTH ventral to P3 (see Qi and Kaas 2006). **b** Dark-field photomicrograph of the adjacent section shows axonal terminations (*arrowheads*) in the GrN after B-HRP was injected into matching locations of P3 and PTH in both feet. **c** Alignment of the two adjacent sections shows the locations of B-HRP-labeled terminations (*blue shading*) overlapping the architectural structure revealed by CO. The label from P3 and PTH injections are next to the CO-dense patches representing the toes (*gray shading*) with the label from PTH ventral (on the *right*) and lateral (on the *left*) to the label from P3. CuN cuneate nucleus, GrN gracile nucleus. Scale bar in **a** is 1 mm and applies to **a–c**

more dorsal patches for P3. Our quantification of the areal extents of the labeled patches (Fig. 5b) indicates that the overall amount and the rostrocaudal distributions of label were similar on both sides, with most of the label in the middle sections. The more caudal extension of the labeled pattern for the left GrN, together with the more rostral extensions of the patterns for the right GrN is consistent with the histological evidence (Fig. 4a) that the left nucleus was slightly more caudal than the right nucleus in each section. Also, we found that the distribution of the relative intensities of labeled patterns was very similar for both gracile nuclei (Fig. 5c). We conclude that the injections on

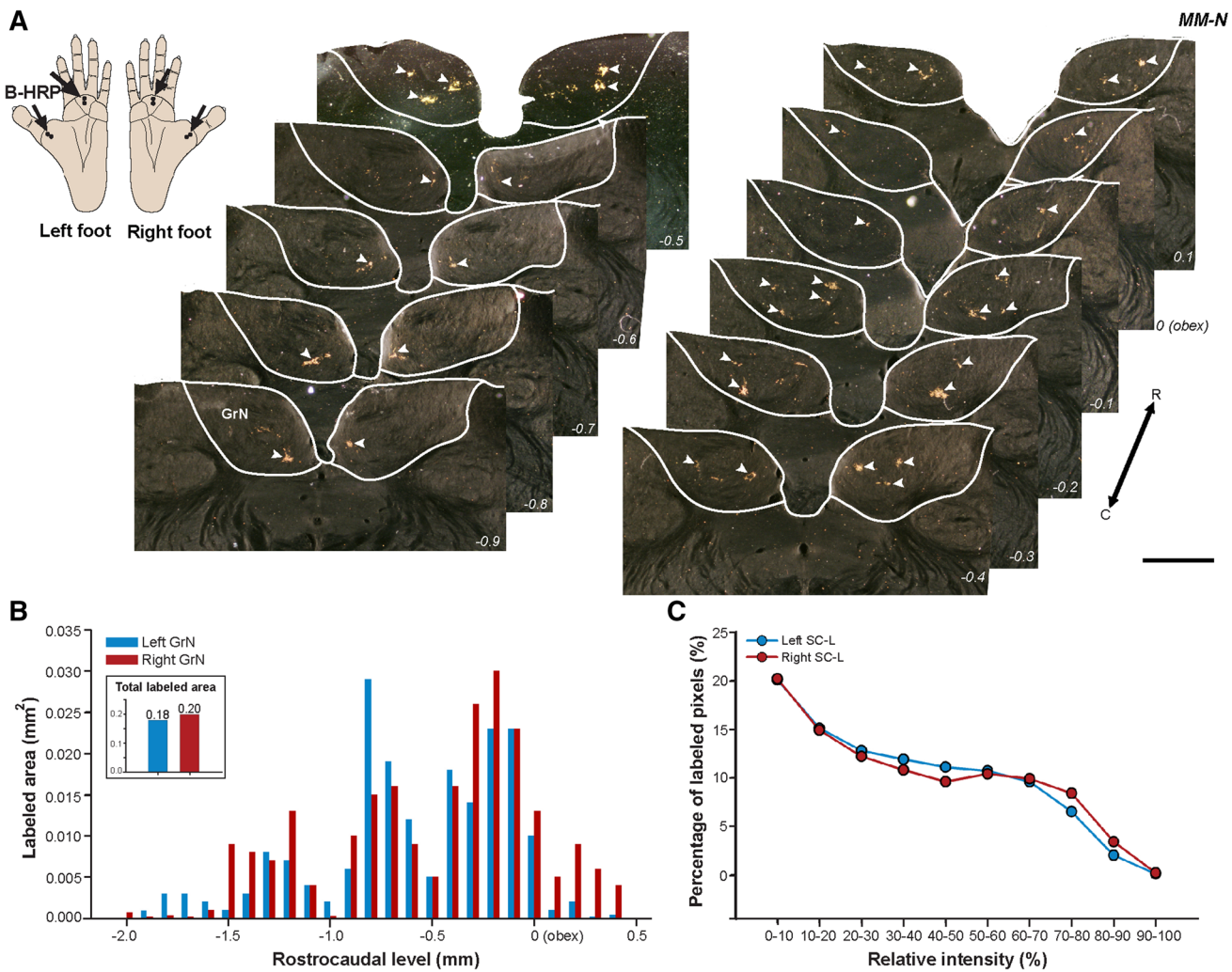


Fig. 5 Axonal terminations in the GrN labeled by subcutaneous B-HRP injections in P3 and PTH on both feet of a normal macaque monkey (MM-N) show typical topographic organization through the rostrocaudal extent of the GrN. **a** Dark-field photomicrographs of coronal sections show the B-HRP-labeled terminals (arrowheads) in the GrN on the two sides. The B-HRP-labeled patches slightly rotated along the rostrocaudal extent of the nucleus with the ventral and medial patches for PTH and the more dorsal patches for P3. **b** Bar

graphs show the areal extents of B-HRP-labeled fields in the GrN on the two sides across the rostrocaudal series of sections. The total labeled areal size is 0.18 mm^2 on the left side and 0.20 mm^2 on the right side, and no significant differences in the extents of B-HRP-labeled fields were detected in the two sides of gracile nuclei ($P = 0.1133$). **c** Curve diagram shows that the percentages of the relative intensities of labeled pixels in the GrN on the two sides are similar ($P = 0.8652$). Scale bar in **a** is 1 mm

both feet were similar and that the foci transported label in GrN were similar on both sides.

In monkey MM-D with the deformed left foot, the GrN appeared to be somewhat abnormal on both sides of the brainstem. In brain sections processed for CO (Fig. 6a), the pattern of CO-dense clusters less clearly matched the normal patterns seen in case MM-N, and appeared to be disordered and different on the two sides. The arrangement of VGLUT2-dense patches, which reflect the terminations of dorsal column afferents (Liao et al. 2013), also showed these differences. In the right GrN, with inputs from a normal appearing foot, multiple patches of labeled axons were apparent in approximately normal dorsal and ventral

locations for the P3 and PTH injections, respectively (Fig. 6c, d). These patches rotated slightly in caudal GrN (Fig. 7). Labeled patches of axons in roughly these two locations were also apparent in the left GrN, the side corresponding to the deformed foot without toes (Fig. 6). However, the dorsal patch region, presumptively for P3, contained several small patches, and was more spread out than expected, while the more ventral PTH patch was larger than expected. The P3 patch rotated ventrally in caudal GrN (Fig. 7). As in the normal monkey, the labeled patterns of terminations occupied a smaller area caudally in GrN, and a larger area near the obex (Fig. 7). The patterns of label for the left deformed foot were larger overall than

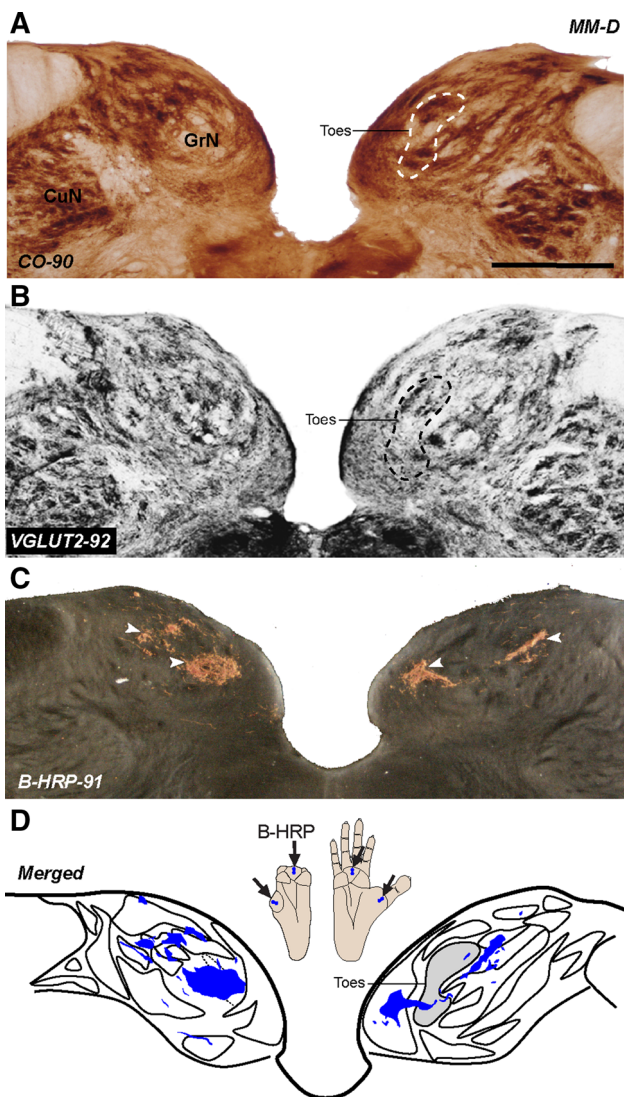


Fig. 6 Photomicrographs of a macaque monkey with a deformed foot (MM-D) illustrate abnormal topographic organization of the foot representation in the GrN. Photomicrographs of adjacent coronal sections reacted for CO (**a**) and vesicular glutamate transporter 2 (VGLUT2; **b**) show the architectural structure in the GrN. The CO- and VGLUT2-dense patches in the medial region of the GrN corresponding to the representations of the toes are apparent on the right side (dashed outline) but appear to be not obvious on the left side. The patches in the lateral region of GrN on the two sides correspond to the representations of the plantar pads. **c** Dark-field photomicrograph of the adjacent section shows the axonal terminations (arrowheads) after B-HRP was injected into matching locations of the P3 and PTH in both feet. Several patches of B-HRP-labeled terminals are in dorsolateral and ventromedial locations, respectively, for P3 and PTH on the two sides, but the B-HRP-labeled fields are more widely distributed and occupy an overall larger area on the left side. **d** Superimposing the B-HRP-labeled section and the adjacent VGLUT2 section shows the locations of B-HRP terminations (blue shading) overlapping the VGLUT2-revealed architecture. Note that the B-HRP-labeled terminals on the right side are scarcely overlapping VGLUT2-dense ovals representing the toes, whereas the labeled terminals on the left side expand into the medial aspect of GrN, overlapping the matching location for toes. Scale bar in **a** is 1 mm and applies to **a–c**

those for the normal appearing foot, suggesting a greater spread of the terminals (Fig. 7b). The relative intensities of labeled patterns were similar on both sides (Fig. 7c) and not that much different from those for the normal monkey (Fig. 5c).

The arrangement and extent of foci of labeled axon terminals in GrN after the PTH and P3 injections in the feet of the two monkeys can be more easily compared in Fig. 8 when the sections through the left GrN are reversed to match the orientations of the right GrN. In the normal GrN, each of the two injections produced several small, closely aligned patches in most sections. Tentatively, we can align one group of patching to the PTH injection and the other group to the P3 injection. Because two closely spaced injections were placed in each pad, this might account for some, but not all of the patchy arrangement (Qi and Kaas 2006). Also there may be more divergence and convergence of inputs for some clusters of neurons in GrN than others, especially more rostrally in the nucleus near the obex. The more medial and ventral patches likely correspond to the PTH injections. The injections in the deformed foot with missing toes were also placed in PTH and P3, but the spread of labeled patches of terminals was clearly greater than in the normal monkey, especially near the obex, and some of this spread likely included the part of GrN that normally represents the toes. Yet some topography in the projection pattern seems to be preserved. The injections in the normal-appearing foot of MM-D produced patches of labeled axons that were more normal in distribution, but they also seemed more scattered than expected, possibly overlapping the toe representational territory medially in GrN, and laterally near the obex into possibly lower leg and ankle territory.

In summary, in all four nuclei, the PTH and P3 injections labeled several patches of labeled axon terminals, making a precise identification of the assignment of patches to skin territories somewhat uncertain, but a comparison with previous results (Qi and Kaas 2006) would suggest that more medioventral patches resulted from the PTH injections in the normal monkey. The label for the deformed foot was more widely distributed, providing evidence that terminals included parts of GrN normally devoted to toes and possibly other parts of the nucleus. The projections from the normally appearing foot were overall more normal in appearance, but they appeared to be somewhat more widespread within the nucleus.

Thalamus

The ventroposterior nucleus of the somatosensory thalamus relays inputs from the contralateral dorsal column-trigeminal complex to primary somatosensory cortex

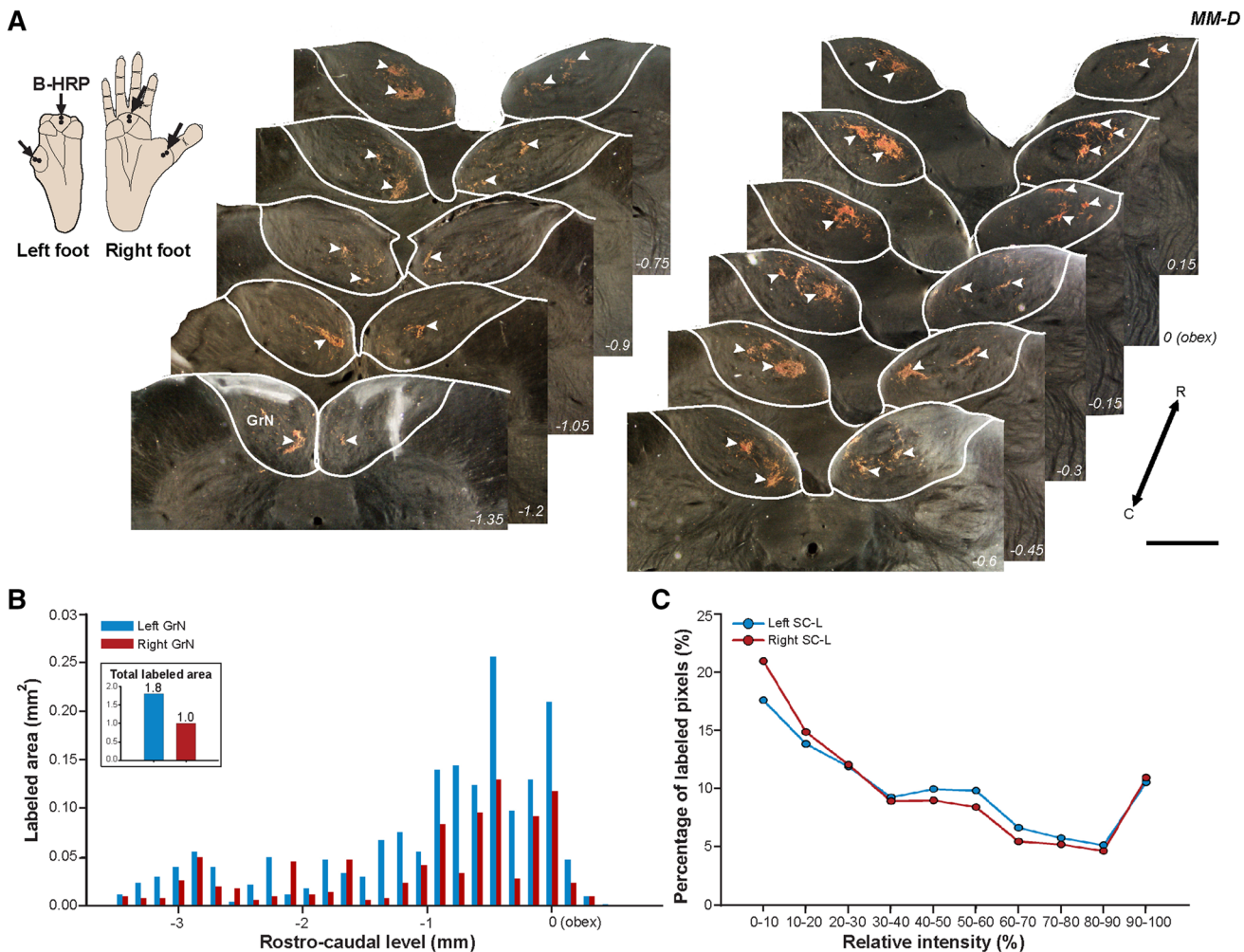


Fig. 7 Axonal terminations in the GrN labeled by subcutaneous B-HRP injections in P3 and PTH on both feet of a macaque monkey with a deformed left foot (MM-D) show abnormal topographic organization through the rostrocaudal extent of the GrN. **a** Dark-field photomicrographs of coronal sections show the B-HRP-labeled terminals (arrowheads) in the left and right gracile nuclei. Two or more patches of the B-HRP-labeled terminals are in the medioventral and lateral locations on the two sides along the rostrocaudal series of sections. The B-HRP-labeled fields on the *left* side are expanded and

more distributed overall, especially near the obex. **c** Bar graphs show the areal extents of B-HRP-labeled fields in the GrN on the two sides across the rostrocaudal series of sections. The total labeled areal size is 1.8 mm² on the *left* side and 1.0 mm² on the *right* side. The extent of B-HRP-labeled fields is significantly expanded in the left GrN (*P < 0.0001). **d** Curve diagram shows that the percentages of the relative intensities of labeled pixels in the gracile nuclei on the two sides are similar (P = 0.5566). Scale bar in **a** is 1 mm

(area 3b) in a topographic manner. The nucleus has two traditional subnuclei, the VPL for the lower body, and the ventroposterior medial subnucleus (VPM) for the face and head. Based on the thalamocortical connections, neurons projecting to the foot representation of area 3b are located in the lateral subdivision of the VPL (Lin et al. 1979; Jones et al. 1979; Whitsel et al. 1978; Kievit and Kuypers 1975; Nelson and Kaas 1981). The representations of toe tips are largely ventral in the VPL, where they are in a mediolateral sequence of toes 1–5 (Kaas et al. 1984). The representation of the proximal leg is dorsal and caudal in the VPL.

Normal foot in VPL

To reveal the representation of the toes and plantar foot in VPL in a normal monkey (MM-N), we injected retrograde tracers into representations of toes and plantar pads in area 3b. WGA-HRP was injected in cortex representing toes 3 and 4 of area 3b of the left cerebral hemisphere and the representation of toe 3 of area 3b of the right cerebral hemisphere after these representations were identified with microelectrode recordings (Fig. 9). The CTB injections involved the representations of plantar pads of the foot, mainly PTH, in each hemisphere. CTB or WGA-HRP

retrogradely labeled neurons in the thalamus that were related to the hindlimb partition of VPL in coronal sections processed for CO (Fig. 10a–d). Some of the more dorsal of the WGA-HRP labeled neurons in VPL of the left hemisphere could have reflected a slight involvement of the injection core in the representation of P3. The results from the two hemispheres revealed that the representations of the plantar pads are largely dorsomedial and somewhat caudal to the representations of the toes in VPL of normal monkeys (Fig. 10e). In a previous study, somewhat larger injections of the representations of toes or plantar foot in area 3b of macaques produced similar results (Nelson and Kaas 1981).

Normal foot in VPL of abnormal monkey

Similarly, in area 3b of the left hemisphere in MM-D, WGA-HRP was injected into the representation of the toes, and CTB was injected into the representation of the insular plantar pads (PIs) (MM-D; Fig. 11). The labeled neurons were in the lateral “hindlimb” subnucleus of VPL, as expected, with those from the injection in toe cortex rostral and ventral to those from the injection in plantar pad cortex (Fig. 12). No clear difference in the organization of the foot representation in VPL was obvious from the labeled connections in the normal monkey.

Abnormal foot in VPL of abnormal monkey

In area 3b of the right hemisphere in MM-D, CTB was injected into the PIs representation similar to how it was placed in the left hemisphere (Fig. 11). The labeled neurons were again in the “hindlimb” subnucleus in approximately the expected locations for the representation of the plantar pads, but the foci of labeled neurons extended more ventrally into regions expected to represent toes (Fig. 12), suggestive of altered somatotopy in VPL.

In summary, the patterns of thalamocortical connections were similar in both hemispheres in the normal monkey, and in the left hemisphere contralateral to the intact foot of the deformed monkey. The more ventral extension of the labeled neurons in the right hemisphere related to the deformed foot is consistent with the possibility that neurons in the former toe territory of VPL projected to cortex representing the plantar pads.

Cortex

The primary somatosensory area 3b in the macaque monkey is composed of the cutaneous representations of face, forelimb, trunk, and hindlimb in a lateral to medial order (Nelson et al. 1980). In the normal monkey, MM-N, we found the representation of glabrous foot was largely consistent with earlier findings using electrophysiological mapping methods

(Fig. 13). The foot representation of area 3b is located on the dorsal surface of the anterior parietal cortex and extends into the medial wall of the cerebral hemisphere (Fig. 13a). When the microelectrode recordings progressed from lateral to medial, the knee and lower leg representations were first identified followed by representations from tibial to fibular foot. For example, the representations of glabrous toes 1–5 were arranged in a lateral to medial sequence along the rostral aspect of area 3b (Fig. 13b-a'). The distal to proximal compartments of plantar representations, commencing with the P2 and P3 to the PIs and PTH, were sequentially identified caudal to the toe representations (Fig. 13b-b'). The caudal area 1 adjoins the area 3b with a reversal of the foot representation (Nelson et al. 1980). Deep in the medial wall of the parietal cortex, the representations of ankle, lower leg, and knee were sequentially found in both areas 3b and 1 (Fig. 13). Area 3a, just rostral to area 3b, is less responsive to cutaneous stimulation, but it was partly mapped to reveal the expected somatotopy in parallel with that of area 3b.

In the abnormal monkey with a deformed left foot, MM-D, we mapped the foot representations in area 3b of the two hemispheres. The mapping in the left area 3b representing the right, physically intact foot revealed a representation with both normal and abnormal features (Fig. 14). We identified the plantar pads including the heel, PTH, PH, PIs, and P2 on the dorsal surface of parietal cortex as expected. The toes were represented rostral and medial to the plantar pads, extending into the medial wall of the longitudinal fissure. Although the representations changed from the tibial to fibular sides when the microelectrode was moved toward the midline on the lateral surface, we found that representation of the glabrous skin and the dorsal parts of toes 1–5 were irregular and disorderly on the medial surface of area 3b (see example in Fig. 14b-a'). The representation of the plantar pads, which were expected to be located caudal to the toes in area 3b, was instead intermingled with that of the toes. However, the representations of ankle, knee, leg, and thigh were encountered as expected when the recording sites were deeper than the foot representation in the cortex of medial wall. In addition, the expected reversal of somatotopy of plantar representations in areas 3b and 1 was observed (Fig. 14b-b'). The receptive fields shifted from the distal toes to the proximal plantar pads in area 3b, and reversed to the plantar pads and toes in area 1, as the microelectrode recordings progressed from rostral to caudal.

Finally, we investigated the representation of the deformed left foot in the right area 3b of monkey MM-D (Fig. 15). The left foot did not have toes 1, 3, and 5, but the most proximal bits of toes 2 and 4, and the plantar pads remained intact. The microelectrode mapping revealed that most neurons in the expected foot representation of area 3b responded to the plantar pad stimulation in a somatotopic manner. We identified the representation of the remaining

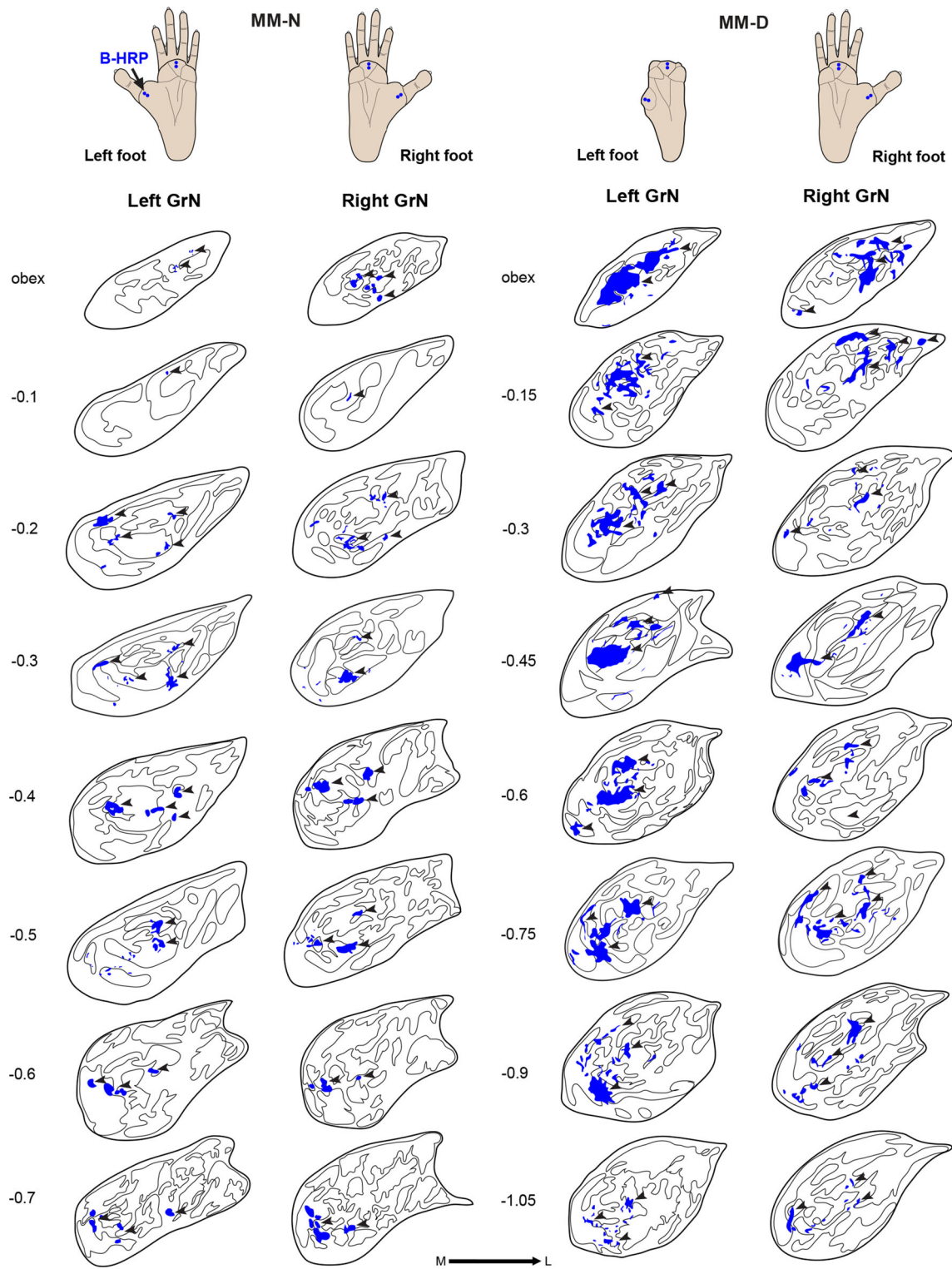


Fig. 8 Patterns of axon terminals in GrN differ after B-HRP was subcutaneously injected into matching locations of the PTH and P3 of both feet in a normal monkey (MM-N) and a monkey with a deformed left foot (MM-D). The left GrN is reversed to match the mediolateral orientation of the right GrN to aid the comparison. The locations of B-HRP-labeled patches are shown in *blue shading* overlapping drawings of the architectural structures revealed by CO- or VGLUT2-staining. In the MM-N, the B-HRP injections produced patches of axon terminals in medioventral and laterodorsal locations on the two sides in a similar pattern along the rostrocaudal series of sections. However, the same amount and locations of B-HRP injections in the deformed left foot of monkey MM-D labeled axon terminals with a greater spread than those in the contralateral GrN that represents the normal appearing foot. Note that labeled patches in the left GrN expand medially into the region that normally represents the toes. *L* lateral, *M* medial. *Numbers* on the *left* indicate the distances (in mm) from the obex, with negative values indicating sections caudal to the obex

glabrous skin of toe 2 in a normal location in the rostral aspect of area 3b on the lateral surface of parietal cortex. However, the representation of distal plantar pads, P2 to P4, expanded to the rostral border of area 3b surrounding the representation of toe 2. The representation of the remaining bit of proximal toe 4 was occasionally encountered adjacent to the representations of the distal pads. In general, the topographic organization of the plantar pads in area 3b was consistent with the foot representation in normal animals. The representations of pads from tibial to fibular were organized in a lateral to medial arrangement (Fig. 15b-a') and the representation of the distal to proximal pad was organized in a rostral to caudal arrangement (Fig. 15b-b', c'). The foot representation of area 1 was organized as a mirror image of the adjoining area 3b where the proximal pad representation was located. However, the representations of toes were of course missing, and the cortical territory of the toes in area 3b appeared to be largely occupied by an expanded representation of the plantar foot, although little of the representation of the preserved part of toe 2 was found on the medial wall. Receptive fields were within the normal range of sizes (Fig. 15).

In summary, the cortical representation of the deformed foot with the missing toes was abnormal in that toe representations were missing. As expected, the cortical territories were activated by an expanded representation of the plantar foot. Quite unexpectedly, the representation of the intact foot in the left hemisphere was also abnormal in that the representations of toes were disorganized compared to the normal monkey.

Discussion

In the present study, we were able to determine important aspects of the organization of the somatosensory system of

an adult monkey with a congenital failure of toe development on one foot, except for small nubs of toes 2 and 4. Of course, we thought that the portions of the somatosensory system that would normally represent inputs from the missing toes would be included in an expanded plantar surface of the foot and that the central nervous system representations of the apparently normal foot would be free of abnormalities, but our suppositions were not completely correct. Here we consider these results from spinal cord to cortex.

When we injected tracers into the PTH and P3 of the deformed foot and the other normal appearing foot, as well as in these locations in each foot of a normal control monkey, we found that the terminations of afferents from these locations in the dorsal horn of the lumbar spinal cord were spread out along the length of the spinal cord in an almost continuous manner, in contrast to the segregated loci observed in the normal monkey. Thus, the inputs from the pads of the foot with missing toes spread out to possibly replace missing inputs from the missing toes (Koerber et al. 1993; Brown and Fuchs 1975). Unexpectedly, these inputs also spread out, although to a more limited extent, from the other foot with intact toes. Such a spread of inputs from the foot with missing toes was expected, as a spread to vacant dorsal horn territories also occurs in adult monkeys from preserved parts of injured forelimbs after long-standing amputations for therapeutic reasons (Florence and Kaas 1995; Wu and Kaas 2002). However, the spread of inputs in the dorsal horn from the normal-appearing foot differed from those in a normal control monkey, and this unexpected spread occurred with inputs from intact toes although this innervation may have been less abnormal. The two sides of the spinal cord are known to communicate through spinal commissural interneurons and dorsal horn neurons with commissural axons (Petko et al. 2004), and it is possible that these commissural influence results in more matching pattern at peripheral nerve inputs on the two sides of the spinal cord.

The other branches of peripheral nerve inputs from the foot ascend in the dorsal column to the GrN. In a central zone in this nucleus (pars rotunda), inputs from the different parts of the foot and hindlimb terminate on specific cell clusters that densely express CO (Qi and Kaas 2006). These CO-dense clusters of neurons are also revealed by concentrations of the VGLUT2 in axon terminations as we show in Fig. 5. CO-dense and VGLUT2-dense features were seen not only in the GrN of the normal monkey studied here, but also in both nuclei of the monkey with missing toes on the left foot (Fig. 5). Thus, there was nothing remarkably abnormal about either the histology or the termination patterns of the inputs from the PTH or P3 in the GrN related to the normal appearing foot or the deformed foot. The widespread peripheral nerve terminations in the dorsal horn of the lumbar spinal cord were

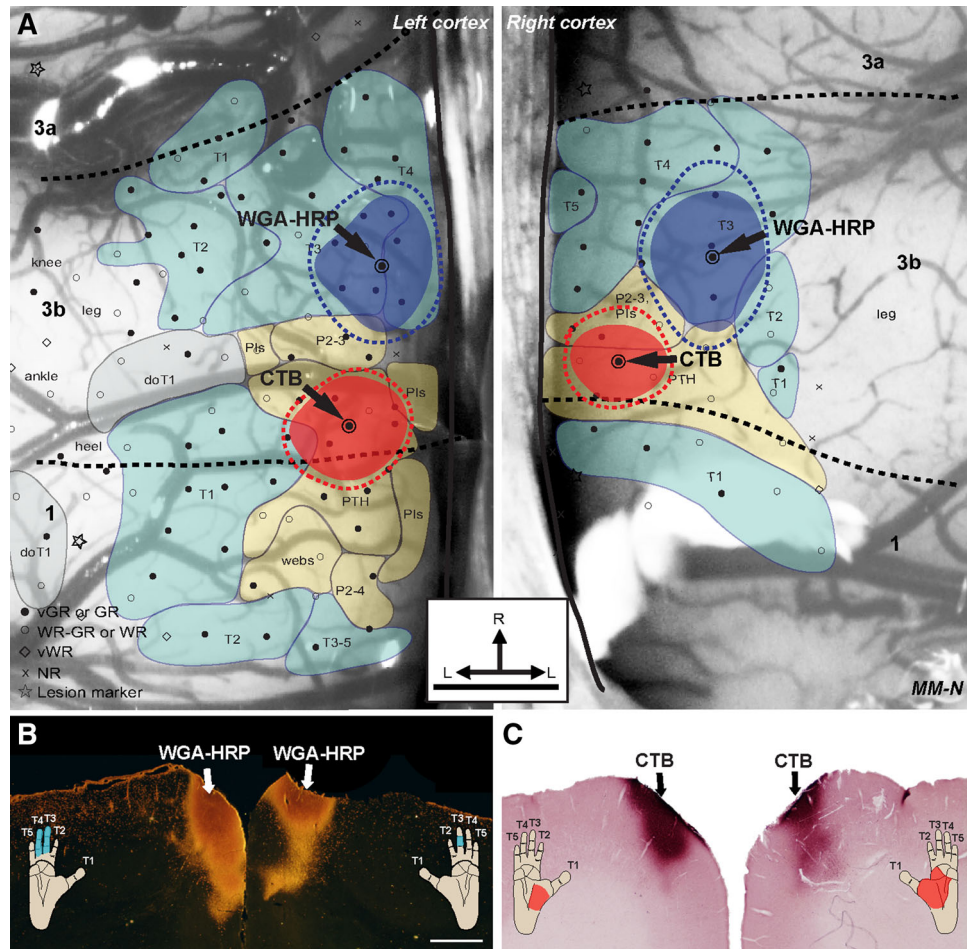


Fig. 9 Locations of tracer injections into electrophysiologically mapped regions of the foot representation in primary somatosensory cortex are depicted in a normal macaque monkey (MM-N). **a** Illustrations overlaid on photographs from the dorsal surface of somatosensory cortex in the left and right hemispheres depict topographic maps and the locations of tracer injections. Black symbols mark the locations of microelectrode penetrations. The representations of toes are shaded in green and the representations of plantar pads are shaded in yellow. The gray shading depicts the dorsal part of foot. The representations of toes from tibial to fibular in area 3b are arranged in a lateral to medial sequence, with tips of the toes located rostrally and the plantar pad located caudally. The foot representation in area 1 adjoins the plantar representation in area 3b caudally with a reversed somatotopy. Neuronal responsiveness was classified into very good response or good response (vGR or GR), weak to good response or weak response (WR-GR or WR), very weak response (vWR) and no

response (NR). The estimations of areal borders of areas 3b and 1 (black dashed lines) were made according to the response modalities and reversed foot representations. Wheat germ agglutinin horseradish peroxidase (WGA-HRP) was injected into the representations of toes 3 and 4 (blue shading) and cholera toxin B subunit (CTB) was injected into the representation of plantar pads, mainly PTH (red shading), in the left area 3b. In the right area 3b, WGA-HRP was injected into the T3 representation and CTB was injected into the representations of PTH and PIs. Blue and red dashed lines show the extents of tracer spread. **b, c** Photomicrographs of coronal sections show the WGA-HRP and CTB injection sites in area 3b of left and right hemispheres. The blue (**b**) and red (**c**) shadings on the drawings of the feet depict the receptive fields of micropipette penetration sites for WGA-HRP and CTB injections. doT1 dorsal toe 1, L lateral, M medial, R rostral, T1–T5 toe 1 to toe 5. Scale bar in **a** is 1 mm; in **b** is 1 mm and applies to **b, c**

simply not seen in the GrN. However, the patchy foci of labeled terminals from the deformed foot were more widely spread in the GrN and appeared to include some of the normal territory for the missing inputs from the toes. An altered somatotopic representation in the GrN was also reported in cats that had one congenitally missing hindfoot in that the nuclear area normally representing the missing part of the hindfoot received inputs from the stump (Schultz et al. 1981). In monkeys with forelimb amputation

as adults, there may be some shrinkage of the CuN, but the nucleus retains the normal appearance of having dark CO patches (Florence and Kaas 1995; Wu and Kaas 2002). Also in these monkeys, there was an expansion of inputs from the intact shoulder or arm into the parts of the nucleus that normally represent the hand. In other cases with a massive loss of dorsal column inputs to CuN of adult monkeys, inputs from the lower face may terminate in the CuN (Jain et al. 2000). Thus, the limited spread of plantar

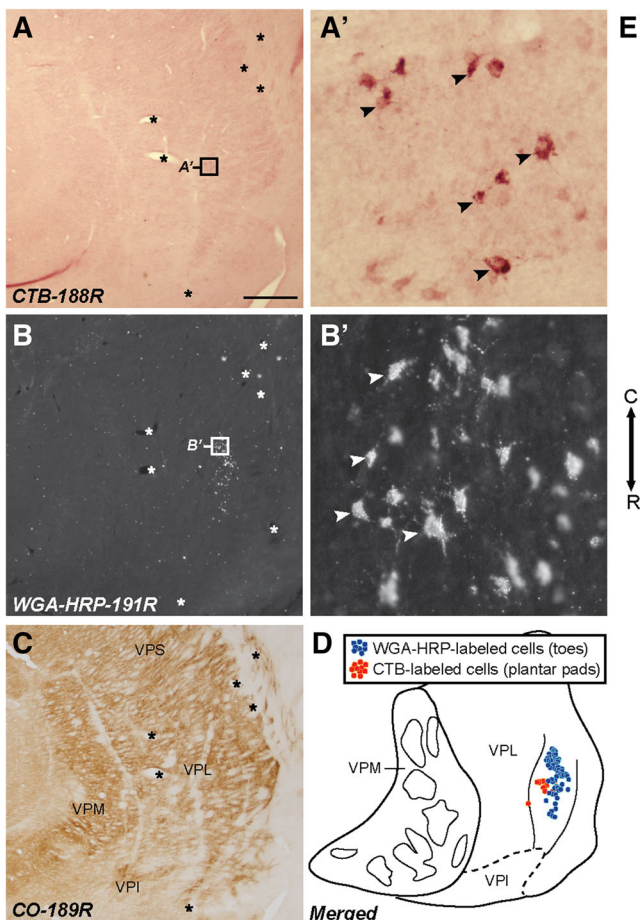


Fig. 10 Distributions of labeled neurons in the thalamus on the *left* and *right* sides show typical and symmetrical patterns after WGA-HRP was injected into the toe representations and CTB was injected into the plantar pad representations in area 3b of both hemispheres of a normal macaque monkey (MM-N, see injection sites in Fig. 9). **a** Photomicrograph of a coronal section shows the locations of CTB-labeled neurons in the ventroposterior lateral nucleus (VPL) on the right side. **b** Dark-field photomicrograph of the adjacent section shows the locations of WGA-HRP-labeled neurons in the VPL. Enlarged (higher magnification) views of labeled neurons (*insets* in **a** and **b**) are shown in **a'** and **b'**. **c** Photomicrograph of the adjacent section shows the structural architecture revealed by the CO reaction. **d** Superimposing adjacent sections shows the locations of the WGA-

HRP- (blue solid circles) and CTB- (red solid circles) labeled neurons overlapping the nuclear architecture revealed by CO in the VPL. The neurons labeled after area 3b injections in parts of the foot representation are located in the lateral region of VPL. **e** A rostrocaudal series of coronal sections shows the WGA-HRP and CTB labeling. Neurons labeled by WGA-HRP injections in toe representations of both cortical hemispheres are located in the region of VPL ventrolateral and rostral to the neurons labeled by CTB injections in representations of the plantar pads. Asterisks in **a**, **b**, and **c** label the landmarks across sections. Arrowheads in **a'** and **b'** indicate labeled neurons. *C* caudal, *VPI* ventroposterior inferior nucleus, *VPM* ventroposterior medial nucleus, *r* rostral. Scale bar in **a** is 1 mm to **a-c** and is 50 μ m to **a', b'**

pad inputs in the GrN seen here as a result of a failure of toe development is something that can also occur in adult monkeys after a sensory loss.

In our two monkeys, we explored the somatotopic organization of the VP nuclei by injecting tracers into the cortical representations of plantar pads and toes to retrogradely label thalamic neurons. For both the nucleus related to the deformed foot and the nucleus related to the apparently normal foot, the distributions of labeled neurons in the ventroposterior nuclei were very similar to those from the comparable cortical injections in our control monkey. In all four cerebral hemispheres, the

thalamic distributions of labeled neurons corresponded closely to the territory representing the foot in the hindlimb subnucleus of VP, as revealed in previous studies (Jones and Friedman 1982; Mayner and Kaas 1986; Mountcastle and Henneman 1952; Nelson and Kaas 1981; Poggio and Mountcastle 1963; Pubols 1968; Loe et al. 1977). However, the patches of labeled neurons extended more ventrally in the hindlimb subnucleus for the deformed foot, suggesting that the ventroposterior territory for both the missing toes and the plantar pads also projects to cortex representing the plantar pads. The ability of the VP to reorganize after a sensory loss to

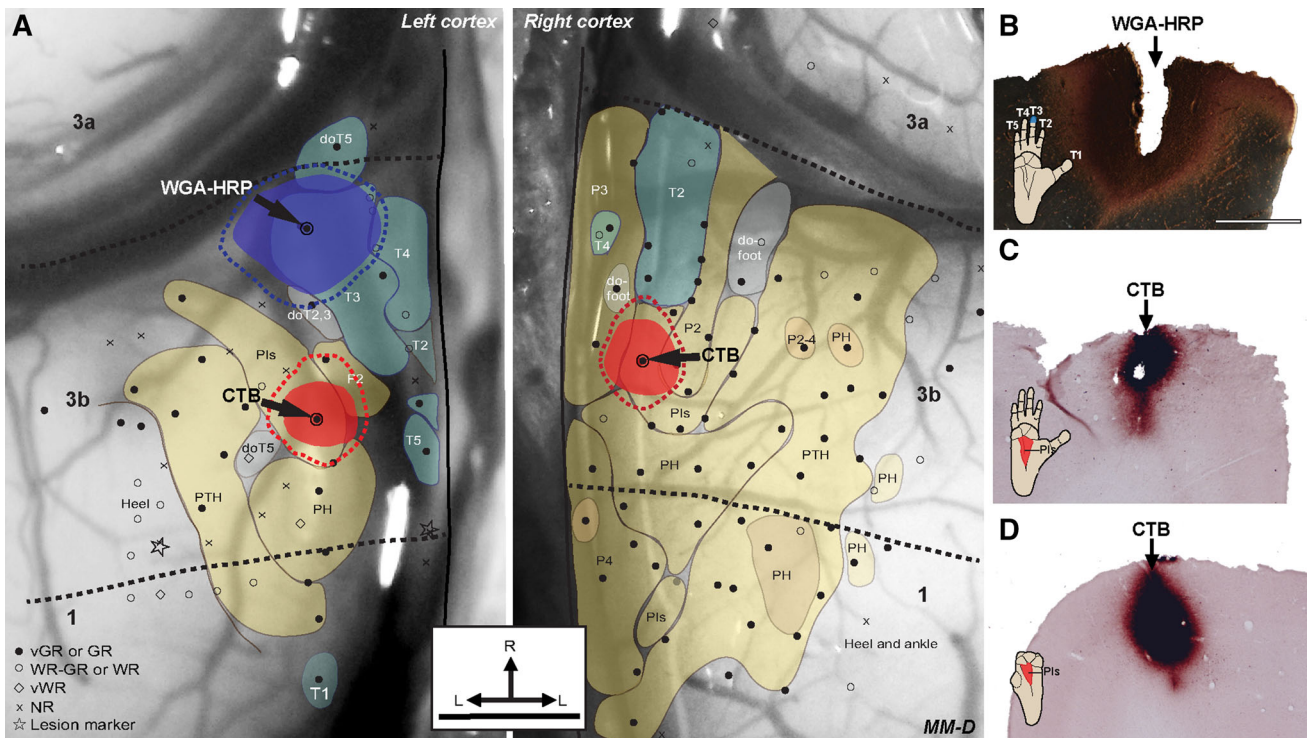


Fig. 11 Tracer injections into electrophysiologically mapped regions of the foot representation in primary somatosensory cortex are depicted in a macaque monkey with a deformed left foot (MM-D). **a** Illustrations overlaid on photographs from the dorsal surface of somatosensory cortex in the left and right hemispheres show the recording sites and locations of tracer injections. In the left area 3b, the representations of toes from tibial to fibular are generally arranged in a lateral to medial sequence but the representations of toes 2 and 5 are also identified caudally. In the right area 3b, the representations of the nubs of toes 2 and 4 are located rostrally and surrounded by the representations of distal plantar pads. The representations of plantar

pads are located caudally and adjoin the caudal area 1 with a reversed somatotopy on the two sides. WGA-HRP was injected into the T3 representation in the left area 3b and CTB was injected into the PIs representation of area 3b on the two sides. **b, c** Photomicrographs of coronal sections show the WGA-HRP and CTB injection sites in the left hemisphere. **d** Photomicrograph of a coronal section shows the CTB injection site in the right hemisphere. The blue (**b**) and red (**c, d**) shadings on the drawings of feet depict the receptive fields of micropipette penetration sites for WGA-HRP and CTB injections. Scale bar in **a** is 1 mm; in **b** is 1 mm and applies to **b–d**. Other conventions are the same as in Fig. 9

reactivate activity-depressed parts of the nucleus with preserved sensory inputs also occurs in adult monkeys (Florence et al. 2000; Garraghty and Kaas 1991; Jain et al. 2008; Jones and Pons 1998). Of course some or all of this reorganization may be relayed from the reorganized dorsal column nuclei, so it is not clear what changes, if any, occur at the level of the thalamus. In consideration of the possibility that the toe representation of the GrN for the deformed foot was innervated by inputs from the plantar skin of the foot, we suggest that projections from the GrN to VPL and then to area 3b all reflect the altered inputs to the GrN to innervate neurons normally innervated by the missing toes.

Finally, we also determined the somatotopic organizations of the foot representation in primary somatosensory cortex, area 3b, as well as less extensively in areas 3a and 1 in cortex representing the deformed foot, and cortex representing the normal foot in the deformed monkey. For comparison, we used microelectrodes to map the foot

cortex of both cerebral cortex in a normal monkey and considered previous mapping results from foot cortex in macaque monkeys (Nelson et al. 1980). The representation of the foot in each hemisphere in our control monkey was, as expected, very similar previous reports, with toes represented anteriorly in area 3b from toe 1 to toe 5 in a lateromedial sequence, and footpads along the area 1 border. The organization in area 1 approximated a mirror reversal of this order. The representation in area 3a was less apparent, but at least it was in parallel with that of area 3b. In the cortex representing the deformed foot of MM-D, the foot cortex was fully activated by the intact portions of the foot so that representations of foot pads extended across the width of area 3b into cortex normally activated by stimulating the toes, although small representations of the remaining nubs of toes 2 and 4 activated small territories in the foot region of area 3b, as well as in area 1. In addition, the overall foot representation was somewhat disordered, such that spatially segregated regions in cortex were

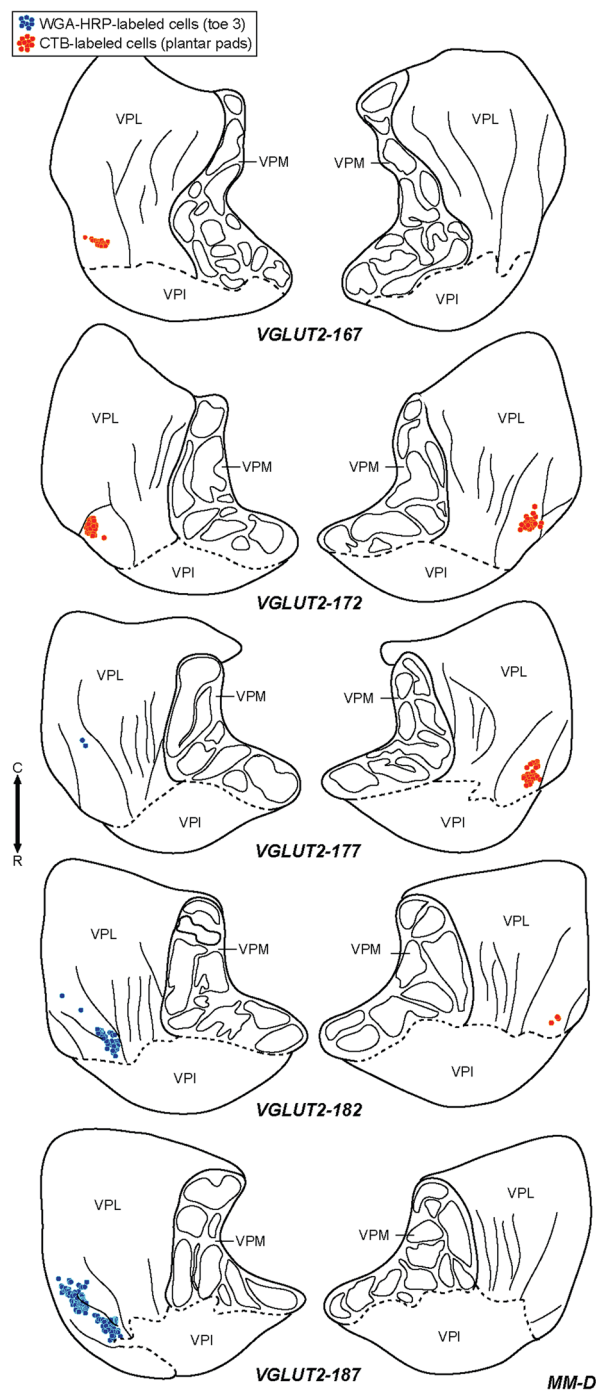


Fig. 12 Drawings from a rostrocaudal series of coronal sections show the asymmetric distributions of labeled neurons in the thalamus after WGA-HRP was injected into the T3 representation in the left area 3b and CTB was injected into the plantar pad representations in area 3b of both hemispheres of the monkey MM-D (see injection sites in Fig. 11). Locations of the label were reconstructed by superimposing the WGA-HRP and CTB processed sections and the adjacent VGLUT2 sections. In the left VPL, the WGA-HRP-labeled neurons (blue solid circles) are located rostral and ventral to the CTB-labeled neurons (red solid circles). The CTB-labeled neurons in the right VPL are in the approximately matching locations but expand to more ventral locations (see sec 182). Other conventions as in Fig. 10

activated by touch on toe nubs and plantar foot surfaces. In cortex reorganized after an extensive sensory loss as adults in monkey, a similar expansion of the representations of preserved inputs occurs (e.g. Bowes et al. 2013; Qi et al. 2013), including the activation of hand and arm cortex by inputs from the face (e.g. Jain et al. 2008; Pons et al. 1991). In addition, in such reactivated cortex, some disorder occurred in that separate regions of cortex sometimes represented the same body part, and the normal somatotopic order was not preserved. This could be explained by the sprouting and growth of new connections at one or more levels of the somatosensory system, mixing in regions of reactivated cortex with regions normally responsive to preserved inputs.

The major puzzling finding was the abnormal somatotopy of the representation of the normal appearing foot in somatosensory cortex of the deformed monkey MM-D. As the toes were present on the right foot of this monkey, the toes were represented in contralateral area 3b as would be expected (Fig. 14), but not in the normal orderly manner we predicted (Fig. 13). Instead, individual toes were represented several times in abnormal locations, above and beyond the normal lateromedial sequence for toes 3–5. The expected large territory for toe 1 on the dorsal surface was largely occupied by representations of plantar pads. We find it difficult to explain this abnormal cortical organization, especially in view of the nearly normal somatotopy of inputs from the normal appearing foot at the level of the GrN and VPL. However, at the cortical level, there would be direct interaction between the foot representations in areas 3b of each hemisphere via the corpus callosum. Although these connections would be sparse in adult monkeys (Killackey et al. 1983), they would be much more dense in prenatal and newborn monkeys (Beck and Kaas 1994; Chalupa and Killackey 1989; Killackey and Chalupa 1986). In addition, there are feedback connections from areas 1 and 2, which contain more dense callosal connections, to area 3b to provide another source of interhemispheric interactions (Pons and Kaas 1986). Potentially, the conflicting patterns of callosal and thalamic inputs could result in abnormal cortical organization in the representation of the normal-appearing foot. In mature macaque monkeys, sensory loss that alters cortical organization in one cerebral hemisphere also results in changes in the other cerebral hemisphere (Calford and Tweedale 1990). In addition, neurons in area 3b of monkeys have receptive fields on the contralateral hand that are partly suppressed by stimuli to the ipsilateral hand (Reed et al. 2011), demonstrating interhemispheric interactions in area 3b. Other possibilities include disrupted molecular guidance factors (Gierer and Muller 1995; Sperry 1963) and altered use-dependent plasticity (Buonomano and Merzenich 1998; Jones 2000).

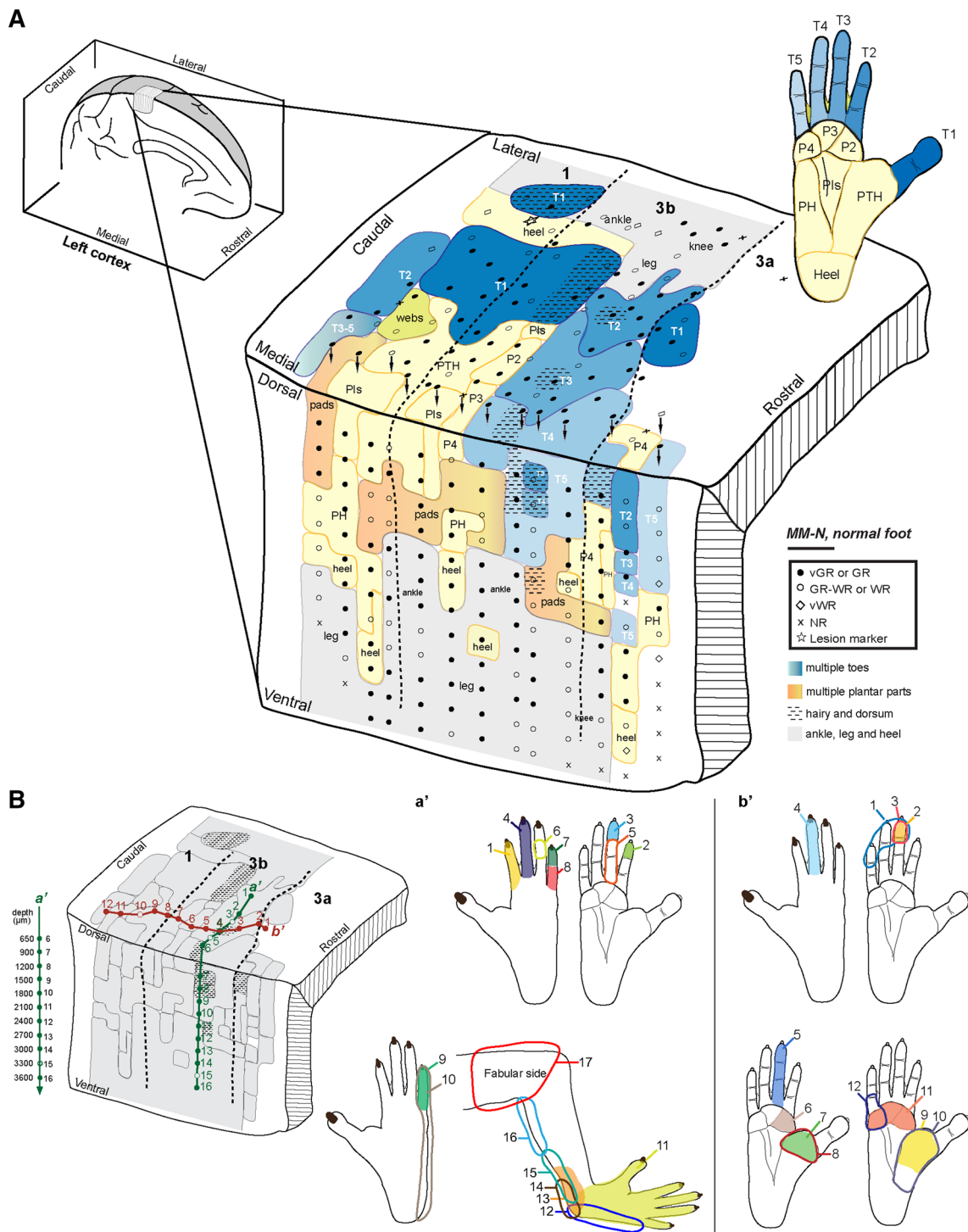


Fig. 13 Cortical somatotopy and receptive fields show typical foot organization in a normal macaque monkey (MM-N). **a** Color-coded pseudo-3D view of a somatotopic map illustrating the foot representation in the left hemisphere. The representations of toes 1–5 are designated in shades of blue from dark to light and the representations of plantar pad are shown in shades of yellow. The representations of the toe webs are shaded in green and the body representations proximal to the foot, including the ankle, leg, knee, and thigh, are shaded in gray. The representations of the dorsal, hairy parts are

shown with shading that overlays the color representing the given body part. In the area 3b, the foot representation is in a somatotopic manner in that representations of glabrous toes 1–5 are arranged in a lateral to medial sequence on the dorsal surface and deep into the medial wall in area 3b. The representations of plantar pads are caudal to the representations of toes and adjoin the area 1 with a reversed plantar representation. **b** Examples of shifts of receptive fields along the lateromedial (a') and rostrocaudal (b') directions. Scale bar in **a** is 500 µm. Other conventions are the same as in Fig. 9

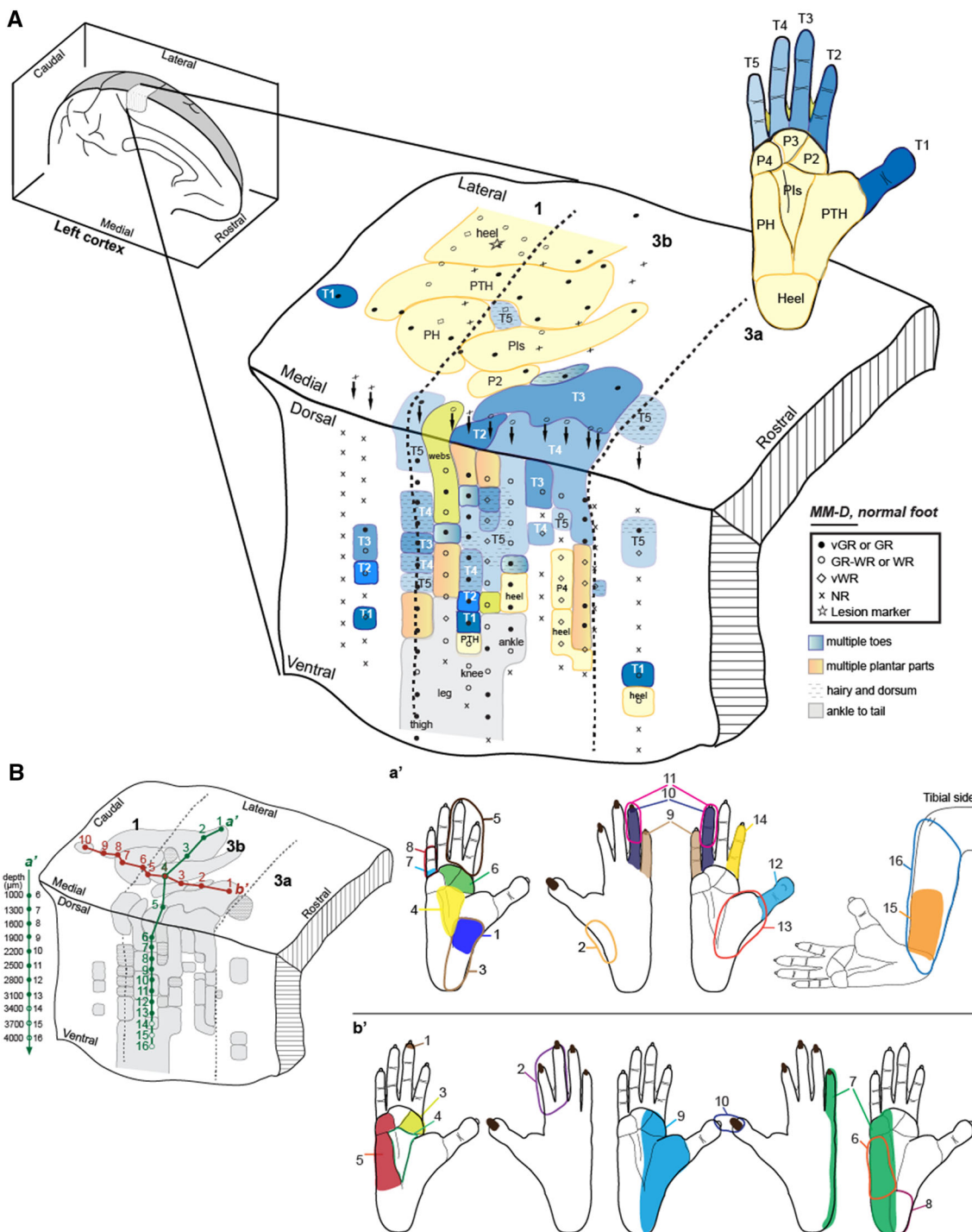


Fig. 14 Cortical somatotopy and receptive fields show abnormal foot organization in the left hemisphere representing the normal appearing right foot of a macaque monkey with a deformed left foot (MM-D). **a** Color-coded pseudo-3D view of a somatotopic map illustrates the right foot representation in the left hemisphere. The representations of toes and plantar pads on the dorsal surface are in a roughly somatotopic organization with the plantar representations in area 3b

are caudal to the toe representations and adjoin area 1 with a reversed plantar representation. In the medial wall of area 3b, the representations of dorsal parts of toes and plantar pads are intermingled disorderly. **b** Examples of shifts of receptive fields along the lateromedial (a') and rostrocaudal (b') directions. Scale bar in **a** is 500 μm. Other conventions are the same as in Fig. 13

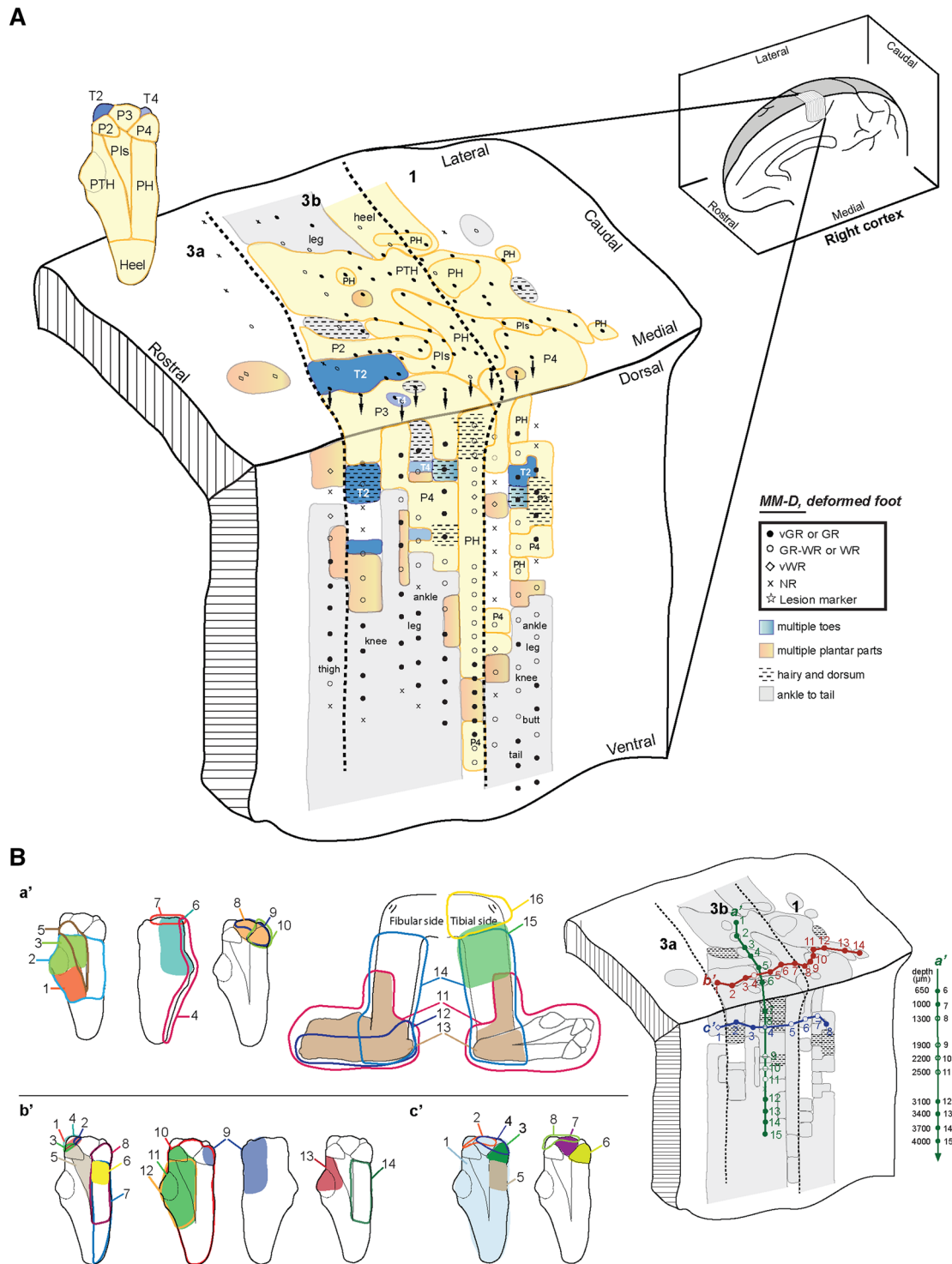


Fig. 15 Cortical somatotopy and receptive fields show abnormal foot organization in the right hemisphere representing the deformed left foot of a macaque monkey (MM-D). **a** Color-coded pseudo-3D view of a somatotopic map illustrates the representation of the deformed left foot in the right hemisphere. The representations of the nubs of toes 2 and 4 are located in the rostral locations of area 3b, neighbored by distal plantar representations. The representations of the plantar pads greatly expand in the foot representations of area 3b. The

representations of plantar pads from tibial to fibular are arranged approximately in lateromedial sequence, and distal to proximal plantar pads are approximately arranged in a rostrocaudal sequence. The representations of the nubs of toes 2 and 4 are located in the rostral locations of area 3b, neighbored by distal plantar representations. The representations of the plantar pads greatly expand in the foot representations of area 3b. The

Relationship to humans with limb malformations

Our results from a single monkey with congenital toe development failure on one foot provides evidence that the cortical representation of that foot was abnormal in that the preserved inputs from the plantar surface of that foot had expanded to occupy the territory normally activated by the missing toes, producing some disorganization. Abnormalities in the VP and GrN were less marked, but likely present. The peripheral nerve inputs from the plantar foot to the dorsal horn of the spinal cord were clearly abnormal as they spread to the presumptive territories of the toes. Surprisingly, there was also a spread of inputs to the dorsal horn of the spinal cord from the plantar foot of the normal-appearing foot, even though the inputs from the intact toes were likely present. The many studies of the somatosensory system in monkeys after various types of sensory loss as adults indicate that the growth of new connections to replace missing or deactivated connections is typical (Darian-Smith 2004; Darian-Smith and Gilbert 1994; Jain et al. 2000; Hickmott and Steen 2005), including the activation of hand cortex, and even the hand portion of the CuN and VP after the extensive loss of hand and arm sensory inputs by inputs from parts of the lower face (Florence et al. 2000; Jain et al. 1997; Pons et al. 1991). Thus, the changes in the somatosensory system reported here for the loss of a sensory input due to abnormal development are somewhat similar to those that have been reported after sensory loss in adult monkeys, and the common mechanism in the replacement of missing inputs is by the sprouting and growth of new connections and other potentiation of preserved sensory inputs (Qi et al. 2014a; Darian-Smith and Ciferri 2006; Bowes et al. 2012).

In cases of extensive sensory loss in adult humans, there is extensive evidence that the somatosensory system reorganizes much as it does in monkeys. Using EEG and fMRI imaging methods in humans after upper limb amputations, there is evidence that the activation of the cortical territory for the lower face expands into lower territory of the hand, much as in monkeys, although this does not always seem to occur (Elbert et al. 1997; Flor et al. 1995). However, it has been difficult to obtain more detailed descriptions of the nature of cortical reorganization after major loss of sensory input with these imaging methods, and it has not been possible to demonstrate alterations in the organization of the somatosensory system at subcortical levels. There have also been studies of cortical organization in humans with congenital malformation of the hand and arm, but these studies are similarly limited by the resolution of the non-invasive imaging methods. In adults with the failure of the upper limb to fully develop, such imaging methods failed to demonstrate that the representation of the lower face expanded into the

territory of the hand in the somatosensory cortex (Flor et al. 1998; Montoya et al. 1998), but these results do not mean that this cortex was not responsive to some other preserved inputs, perhaps from the shoulder, neck or trunk. Other individuals with failure of the hand or fingers to fully develop due to prenatal thalidomide exposure appeared to have reduced presentation of the hand by preserved parts of the hand (Stoeckel et al. 2005a), implying that parts of the territory of the hand representation in cortex were activated by inputs from other parts of the body. When ulnar fingers were present, the ulnar finger representations in the cortex were close to the face region (Stoeckel et al. 2005b), providing further evidence for cortical reorganization within the hand representation. Clearly, more research is needed, as we do not know what findings will be variable or consistent in monkeys or humans with congenital limb malformations, or if changes in somatosensory system organization will relate only to the deformed limb or both limbs.

Acknowledgments This study is supported by National Institutes of Health Grant NS16446 to Jon H. Kaas and National Institutes of Health Grant NS067017 to Hui-Xin Qi. We are grateful to Laura Trice for help with histological procedures and Mary Feurtado for surgical assistance.

Conflict of interest The authors declare that the research was conducted in the absence of any commercial or financial relationships that could be construed as a potential conflict of interest.

References

- Abraira VE, Ginty DD (2013) The sensory neurons of touch. *Neuron* 79(4):618–639. doi:[10.1016/j.neuron.2013.07.051](https://doi.org/10.1016/j.neuron.2013.07.051)
- Angelucci A, Clasca F, Sur M (1996) Anterograde axonal tracing with the subunit B of cholera toxin: a highly sensitive immunohistochemical protocol for revealing fine axonal morphology in adult and neonatal brains. *J Neurosci Methods* 65(1):101–112
- Balaram P, Hackett TA, Kaas JH (2013) Differential expression of vesicular glutamate transporters 1 and 2 may identify distinct modes of glutamatergic transmission in the macaque visual system. *J Chem Neuroanat* 50–51:21–38. doi:[10.1016/j.jchemneu.2013.02.007](https://doi.org/10.1016/j.jchemneu.2013.02.007)
- Beck PD, Kaas JH (1994) Interhemispheric connections in neonatal owl monkeys (*Aotus trivirgatus*) and galagos (*Galago crassicaudatus*). *Brain Res* 651(1–2):57–75
- Blake DT, Byl NN, Merzenich MM (2002) Representation of the hand in the cerebral cortex. *Behav Brain Res* 135(1–2):179–184
- Bowes C, Massey JM, Burish M, Cerkevich CM, Kaas JH (2012) Chondroitinase ABC promotes selective reactivation of somatosensory cortex in squirrel monkeys after a cervical dorsal column lesion. *Proc Natl Acad Sci USA* 109(7):2595–2600. doi:[10.1073/pnas.1121604109](https://doi.org/10.1073/pnas.1121604109)
- Bowes C, Burish M, Cerkevich C, Kaas J (2013) Patterns of cortical reorganization in the adult marmoset after a cervical spinal cord injury. *J Comp Neurol* 521(15):3451–3463. doi:[10.1002/cne.23360](https://doi.org/10.1002/cne.23360)
- Brown PB, Fuchs JL (1975) Somatotopic representation of hindlimb skin in cat dorsal horn. *J Neurophysiol* 38(1):1–9

- Buonomano DV, Merzenich MM (1998) Net interaction between different forms of short-term synaptic plasticity and slow-IPSPs in the hippocampus and auditory cortex. *J Neurophysiol* 80(4):1765–1774
- Calford MB, Tweedale R (1990) Interhemispheric transfer of plasticity in the cerebral cortex. *Science* 249(4970):805–807
- Chalupa LM, Killackey HP (1989) Process elimination underlies ontogenetic change in the distribution of callosal projection neurons in the postcentral gyrus of the fetal rhesus monkey. *Proc Natl Acad Sci USA* 86(3):1076–1079
- Constantine-Paton M, Law MI (1982) The development of maps and stripes in the brain. *Sci Am* 247(6):62–70
- Darian-Smith C (2004) Primary afferent terminal sprouting after a cervical dorsal rootlet section in the macaque monkey. *J Comp Neurol* 470(2):134–150. doi:[10.1002/cne.11030](https://doi.org/10.1002/cne.11030)
- Darian-Smith C, Cifelli M (2006) Cuneate nucleus reorganization following cervical dorsal rhizotomy in the macaque monkey: its role in the recovery of manual dexterity. *J Comp Neurol* 498(4):552–565. doi:[10.1002/cne.21088](https://doi.org/10.1002/cne.21088)
- Darian-Smith C, Gilbert CD (1994) Axonal sprouting accompanies functional reorganization in adult cat striate cortex. *Nature* 368(6473):737–740. doi:[10.1038/368737a0](https://doi.org/10.1038/368737a0)
- Dy CJ, Swarup I, Daluiski A (2014) Embryology, diagnosis, and evaluation of congenital hand anomalies. *Curr Rev Musculoskelet Med.* doi:[10.1007/s12178-014-9201-7](https://doi.org/10.1007/s12178-014-9201-7)
- Elbert T, Sterr A, Flor H, Rockstroh B, Knecht S, Pantev C, Wienbruch C, Taub E (1997) Input-increase and input-decrease types of cortical reorganization after upper extremity amputation in humans. *Exp Brain Res* 117(1):161–164
- Flor H, Elbert T, Knecht S, Wienbruch C, Pantev C, Birbaumer N, Larbig W, Taub E (1995) Phantom-limb pain as a perceptual correlate of cortical reorganization following arm amputation. *Nature* 375(6531):482–484. doi:[10.1038/375482a0](https://doi.org/10.1038/375482a0)
- Flor H, Elbert T, Muhlnickel W, Pantev C, Wienbruch C, Taub E (1998) Cortical reorganization and phantom phenomena in congenital and traumatic upper-extremity amputees. *Exp Brain Res* 119(2):205–212
- Florence SL, Kaas JH (1995) Large-scale reorganization at multiple levels of the somatosensory pathway follows therapeutic amputation of the hand in monkeys. *J Neurosci* 15(12):8083–8095
- Florence SL, Wall JT, Kaas JH (1988) The somatotopic pattern of afferent projections from the digits to the spinal cord and cuneate nucleus in macaque monkeys. *Brain Res* 452(1–2):388–392
- Florence SL, Jain N, Pospischal MW, Beck PD, Sly DL, Kaas JH (1996) Central reorganization of sensory pathways following peripheral nerve regeneration in fetal monkeys. *Nature* 381(6577):69–71. doi:[10.1038/381069a0](https://doi.org/10.1038/381069a0)
- Florence SL, Hackett TA, Strata F (2000) Thalamic and cortical contributions to neural plasticity after limb amputation. *J Neurophysiol* 83(5):3154–3159
- Gabos PG (2006) Modified technique for the surgical treatment of congenital constriction bands of the arms and legs of infants and children. *Orthopedics* 29(5):401–404
- Garraghty PE, Kaas JH (1991) Large-scale functional reorganization in adult monkey cortex after peripheral nerve injury. *Proc Natl Acad Sci USA* 88(16):6976–6980
- Gibson AR, Hansma DI, Houk JC, Robinson FR (1984) A sensitive low artifact TMB procedure for the demonstration of WGA-HRP in the CNS. *Brain Res* 298(2):235–241
- Gierer A, Muller CM (1995) Development of layers, maps and modules. *Curr Opin Neurobiol* 5(1):91–97
- Goldman AS (1980) Critical periods of prenatal toxic insults. In: Schwarz RH (ed) *Drug and chemical risks to the fetus and newborn*. Wiley Liss, New York, pp 9–31
- Hendrickx AG, Prahalada S (1986) Teratology and embryogenesis. In: Dukelow RW (ed) *Comparative primate biology*, vol V. Alan R. Liss Inc, New York, pp 333–362
- Hickmott PW, Steen PA (2005) Large-scale changes in dendritic structure during reorganization of adult somatosensory cortex. *Nat Neurosci* 8(2):140–142. doi:[10.1038/nn1384](https://doi.org/10.1038/nn1384)
- Hubel DH, Wiesel TN (1970) The period of susceptibility to the physiological effects of unilateral eye closure in kittens. *J Physiol* 206(2):419–436
- Jain N, Catania KC, Kaas JH (1997) Deactivation and reactivation of somatosensory cortex after dorsal spinal cord injury. *Nature* 386(6624):495–498. doi:[10.1038/386495a0](https://doi.org/10.1038/386495a0)
- Jain N, Florence SL, Qi HX, Kaas JH (2000) Growth of new brainstem connections in adult monkeys with massive sensory loss. *Proc Natl Acad Sci USA* 97(10):5546–5550. doi:[10.1073/pnas.090572597](https://doi.org/10.1073/pnas.090572597)
- Jain N, Qi HX, Collins CE, Kaas JH (2008) Large-scale reorganization in the somatosensory cortex and thalamus after sensory loss in macaque monkeys. *J Neurosci* 28(43):11042–11060. doi:[10.1523/JNEUROSCI.2334-08.2008](https://doi.org/10.1523/JNEUROSCI.2334-08.2008)
- Jones EG (2000) Cortical and subcortical contributions to activity-dependent plasticity in primate somatosensory cortex. *Annu Rev Neurosci* 23:1–37. doi:[10.1146/annurev.neuro.23.1.1](https://doi.org/10.1146/annurev.neuro.23.1.1)
- Jones EG (2007) The ventral nuclei. In: Jones EG (ed) *The thalamus*, vol 2, 2nd edn. Cambridge, New York, pp 775–795
- Jones EG, Friedman DP (1982) Projection pattern of functional components of thalamic ventrobasal complex on monkey somatosensory cortex. *J Neurophysiol* 48(2):521–544
- Jones EG, Pons TP (1998) Thalamic and brainstem contributions to large-scale plasticity of primate somatosensory cortex. *Science* 282(5391):1121–1125
- Jones EG, Wise SP, Coulter JD (1979) Differential thalamic relationships of sensory-motor and parietal cortical fields in monkeys. *J Comp Neurol* 183(4):833–881. doi:[10.1002/cne.901830410](https://doi.org/10.1002/cne.901830410)
- Kaas JH, Catania KC (2002) How do features of sensory representations develop? *BioEssays* 24(4):334–343. doi:[10.1002/bies.10076](https://doi.org/10.1002/bies.10076)
- Kaas JH, Nelson RJ, Sur M, Dykes RW, Merzenich MM (1984) The somatotopic organization of the ventroposterior thalamus of the squirrel monkey, *Saimiri sciureus*. *J Comp Neurol* 226(1):111–140. doi:[10.1002/cne.902260109](https://doi.org/10.1002/cne.902260109)
- Kaas JH, Qi HX, Burish MJ, Gharbawie OA, Onifer SM, Massey JM (2008) Cortical and subcortical plasticity in the brains of humans, primates, and rats after damage to sensory afferents in the dorsal columns of the spinal cord. *Exp Neurol* 209(2):407–416. doi:[10.1016/j.expneuro.2007.06.014](https://doi.org/10.1016/j.expneuro.2007.06.014)
- Kievit J, Kuypers HG (1975) Subcortical afferents to the frontal lobe in the rhesus monkey studied by means of retrograde horseradish peroxidase transport. *Brain Res* 85(2):261–266. doi:[10.1016/0006-8993\(75\)90079-7](https://doi.org/10.1016/0006-8993(75)90079-7)
- Killackey HP, Chalupa LM (1986) Ontogenetic change in the distribution of callosal projection neurons in the postcentral gyrus of the fetal rhesus monkey. *J Comp Neurol* 244(3):331–348. doi:[10.1002/cne.902440306](https://doi.org/10.1002/cne.902440306)
- Killackey HP, Gould HJ 3rd, Cusick CG, Pons TP, Kaas JH (1983) The relation of corpus callosum connections to architectonic fields and body surface maps in sensorimotor cortex of new and old world monkeys. *J Comp Neurol* 219(4):384–419. doi:[10.1002/cne.902190403](https://doi.org/10.1002/cne.902190403)
- Killackey HP, Rhoades RW, Bennett-Clarke CA (1995) The formation of a cortical somatotopic map. *Trends Neurosci* 18(9):402–407
- Koerber HR, Hobbs G, Brown PB (1993) Precision and variability of hindlimb representation in cat dorsal horn and implications for tactile localization. *J Neurophysiol* 70(6):2489–2501

- Krubitza L, Dooley JC (2013) Cortical plasticity within and across lifetimes: how can development inform us about phenotypic transformations? *Front Hum Neurosci* 7:620. doi:[10.3389/fnhum.2013.00620](https://doi.org/10.3389/fnhum.2013.00620)
- Liao CC, Gharbawie OA, Qi H, Kaas JH (2013) Cortical connections to single digit representations in area 3b of somatosensory cortex in squirrel monkeys and prosimian galagos. *J Comp Neurol* 521(16):3768–3790. doi:[10.1002/cne.23377](https://doi.org/10.1002/cne.23377)
- Lin CS, Merzenich MM, Sur M, Kaas JH (1979) Connections of areas 3b and 1 of the parietal somatosensory strip with the ventroposterior nucleus in the owl monkey (*Aotus trivirgatus*). *J Comp Neurol* 185(2):355–371. doi:[10.1002/cne.901850209](https://doi.org/10.1002/cne.901850209)
- Loe PR, Whitsel BL, Dreyer DA, Metz CB (1977) Body representation in ventrobasal thalamus of macaque: a single-unit analysis. *J Neurophysiol* 40(6):1339–1355
- Lokmane L, Provile R, Narboux-Neme N, Gyory I, Keita M, Mailhes C, Lena C, Gaspar P, Grosschedl R, Garel S (2013) Sensory map transfer to the neocortex relies on pretarget ordering of thalamic axons. *Curr Biol* 23(9):810–816. doi:[10.1016/j.cub.2013.03.062](https://doi.org/10.1016/j.cub.2013.03.062)
- Luo L, Flanagan JG (2007) Development of continuous and discrete neural maps. *Neuron* 56(2):284–300. doi:[10.1016/j.neuron.2007.10.014](https://doi.org/10.1016/j.neuron.2007.10.014)
- Mayner L, Kaas JH (1986) Thalamic projections from electrophysiologically defined sites of body surface representations in areas 3b and 1 of somatosensory cortex of Cebus monkeys. *Somatosens Res* 4(1):13–29
- Merzenich MM, Nelson RJ, Stryker MP, Cynader MS, Schoppmann A, Zook JM (1984) Somatosensory cortical map changes following digit amputation in adult monkeys. *J Comp Neurol* 224(4):591–605. doi:[10.1002/cne.902240408](https://doi.org/10.1002/cne.902240408)
- Montoya P, Ritter K, Huse E, Larbig W, Braun C, Topfner S, Lutzenberger W, Grodd W, Flor H, Birbaumer N (1998) The cortical somatotopic map and phantom phenomena in subjects with congenital limb atrophy and traumatic amputees with phantom limb pain. *Eur J Neurosci* 10(3):1095–1102
- Mountcastle VB, Henneman E (1952) The representation of tactile sensibility in the thalamus of the monkey. *J Comp Neurol* 97(3):409–439
- Nelson RJ, Kaas JH (1981) Connections of the ventroposterior nucleus of the thalamus with the body surface representations in cortical areas 3b and 1 of the cynomolgus macaque, (*Macaca fascicularis*). *J Comp Neurol* 199(1):29–64. doi:[10.1002/cne.901990104](https://doi.org/10.1002/cne.901990104)
- Nelson RJ, Sur M, Felleman DJ, Kaas JH (1980) Representations of the body surface in postcentral parietal cortex of *Macaca fascicularis*. *J Comp Neurol* 192(4):611–643. doi:[10.1002/cne.901920402](https://doi.org/10.1002/cne.901920402)
- Ogino T (2007) Clinical features and teratogenic mechanisms of congenital absence of digits. *Dev Growth Differ* 49(6):523–531. doi:[10.1111/j.1440-169X.2007.00939.x](https://doi.org/10.1111/j.1440-169X.2007.00939.x)
- Padberg J, Krubitza L (2006) Thalamocortical connections of anterior and posterior parietal cortical areas in New World titi monkeys. *J Comp Neurol* 497(3):416–435. doi:[10.1002/cne.21005](https://doi.org/10.1002/cne.21005)
- Petko M, Veress G, Vereb G, Storm-Mathisen J, Antal M (2004) Commissural propriospinal connections between the lateral aspects of laminae III–IV in the lumbar spinal cord of rats. *J Comp Neurol* 480(4):364–377. doi:[10.1002/cne.20356](https://doi.org/10.1002/cne.20356)
- Poggio GF, Mountcastle VB (1963) The functional properties of ventrobasal thalamic neurons studied in unanesthetized monkeys. *J Neurophysiol* 26:775–806
- Pons TP, Kaas JH (1986) Corticocortical connections of area 2 of somatosensory cortex in macaque monkeys: a correlative anatomical and electrophysiological study. *J Comp Neurol* 248(3):313–335. doi:[10.1002/cne.902480303](https://doi.org/10.1002/cne.902480303)
- Pons TP, Garraghty PE, Ommaya AK, Kaas JH, Taub E, Mishkin M (1991) Massive cortical reorganization after sensory deafferentation in adult macaques. *Science* 252(5014):1857–1860
- Pubols BH Jr (1968) Retrograde degeneration study of somatic sensory thalamocortical connections in brain of *Virginia opossum*. *Brain Res* 7(2):232–251
- Qi HX, Kaas JH (2006) Organization of primary afferent projections to the gracile nucleus of the dorsal column system of primates. *J Comp Neurol* 499(2):183–217. doi:[10.1002/cne.21061](https://doi.org/10.1002/cne.21061)
- Qi HX, Chen LM, Kaas JH (2011a) Reorganization of somatosensory cortical areas 3b and 1 after unilateral section of dorsal columns of the spinal cord in squirrel monkeys. *J Neurosci* 31(38):13662–13675. doi:[10.1523/JNEUROSCI.2366-11.2011](https://doi.org/10.1523/JNEUROSCI.2366-11.2011)
- Qi HX, Gharbawie OA, Wong P, Kaas JH (2011b) Cell-poor septa separate representations of digits in the ventroposterior nucleus of the thalamus in monkeys and prosimian galagos. *J Comp Neurol* 519(4):738–758. doi:[10.1002/cne.22545](https://doi.org/10.1002/cne.22545)
- Qi HX, Gharbawie OA, Wynne KW, Kaas JH (2013) Impairment and recovery of hand use after unilateral section of the dorsal columns of the spinal cord in squirrel monkeys. *Behav Brain Res* 252:363–376. doi:[10.1016/j.bbr.2013.05.058](https://doi.org/10.1016/j.bbr.2013.05.058)
- Qi HX, Kaas JH, Reed JL (2014a) The reactivation of somatosensory cortex and behavioral recovery after sensory loss in mature primates. *Front Syst Neurosci* 8:84. doi:[10.3389/fnsys.2014.00084](https://doi.org/10.3389/fnsys.2014.00084)
- Qi HX, Reed JL, Gharbawie OA, Burish MJ, Kaas JH (2014b) Cortical neuron response properties are related to lesion extent and behavioral recovery after sensory loss from spinal cord injury in monkeys. *J Neurosci* 34(12):4345–4363. doi:[10.1523/JNEUROSCI.4954-13.2014](https://doi.org/10.1523/JNEUROSCI.4954-13.2014)
- Rausell E, Bickford L, Manger PR, Woods TM, Jones EG (1998) Extensive divergence and convergence in the thalamocortical projection to monkey somatosensory cortex. *J Neurosci* 18(11):4216–4232
- Reed JL, Qi HX, Kaas JH (2011) Spatiotemporal properties of neuron response suppression in owl monkey primary somatosensory cortex when stimuli are presented to both hands. *J Neurosci* 31(10):3589–3601. doi:[10.1523/JNEUROSCI.4310-10.2011](https://doi.org/10.1523/JNEUROSCI.4310-10.2011)
- Schultz W, Wiesendanger R, Hess B, Ruffieux A, Wiesendanger M (1981) The somatotopy of the gracile nucleus in cats with agenesis of a hindfoot. *Exp Brain Res* 43(3–4):413–418
- Sperry RW (1963) Chemoaffinity in the orderly growth of nerve fiber patterns and connections. *Proc Natl Acad Sci USA* 50:703–710
- Stoeckel MC, Jorgens S, Witte OW, Seitz RJ (2005a) Reduced somatosensory hand representation in thalidomide-induced dysmelia as revealed by fMRI. *Eur J Neurosci* 21(2):556–562. doi:[10.1111/j.1460-9568.2005.03866.x](https://doi.org/10.1111/j.1460-9568.2005.03866.x)
- Stoeckel MC, Pollok B, Witte OW, Seitz RJ, Schnitzler A (2005b) Shrinkage of somatosensory hand area in subjects with upper extremity dysmelia revealed by magnetoencephalography. *J Neurophysiol* 93(2):813–818. doi:[10.1152/jn.00749.2004](https://doi.org/10.1152/jn.00749.2004)
- van der Loos H, Dorfl J (1978) Does the skin tell the somatosensory cortex how to construct a map of the periphery? *Neurosci Lett* 7(1):23–30
- Wall LB, Ezaki M, Oishi SN (2013) Management of congenital radial longitudinal deficiency: controversies and current concepts. *Plast Reconstr Surg* 132(1):122–128. doi:[10.1097/PRS.0b013e318290fca5](https://doi.org/10.1097/PRS.0b013e318290fca5)
- Whitsel BL, Rustioni A, Dreyer DA, Loe PR, Allen EE, Metz CB (1978) Thalamic projections to S-I in macaque monkey. *J Comp Neurol* 178(3):385–409. doi:[10.1002/cne.901780302](https://doi.org/10.1002/cne.901780302)

- Willis WD Jr (2008) Physiological characteristics of sedon order somatosensory circuits in spinal cord and brainstem. In: Basbaum AI, Kaneko A, Shepherd GG (eds) The senses: a comprehensive reference, vol 6. Elsevier, UK, pp 87–110
- Wong-Riley M (1979) Changes in the visual system of monocularly sutured or enucleated cats demonstrable with cytochrome oxidase histochemistry. *Brain Res* 171(1):11–28
- Wu CW, Kaas JH (2002) The effects of long-standing limb loss on anatomical reorganization of the somatosensory afferents in the brainstem and spinal cord. *Somatosens Mot Res* 19(2):153–163. doi:[10.1080/08990220220133261](https://doi.org/10.1080/08990220220133261)